Accepted Manuscript

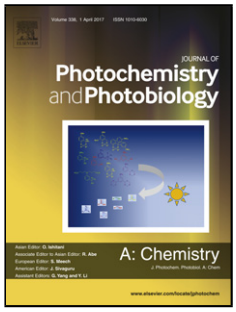

Title: Synthesis of a novel pyrene derived perimidine and exploration of its aggregation induced emission, aqueous copper ion sensing, effective antioxidant and BSA interaction properties

Author: Nilanjan Chakraborty Senjuti Banik Arijit Chakraborty Swapan Kumar Bhattacharya Suman Das

PII: S1010-6030(19)30149-2
DOI: https://doi.org/doi:10.1016/j.jphotochem.2019.03.014
Reference: JPC 11751

To appear in: *Journal of Photochemistry and Photobiology A: Chemistry*

Received date: 24 January 2019
Revised date: 1 March 2019
Accepted date: 7 March 2019

Please cite this article as: N. Chakraborty, S. Banik, A. Chakraborty, S.K. Bhattacharya, S. Das, Synthesis of a novel pyrene derived perimidine and exploration of its aggregation induced emission, aqueous copper ion sensing, effective antioxidant and BSA interaction properties, *Journal of Photochemistry and Photobiology A: Chemistry* (2019), https://doi.org/10.1016/j.jphotochem.2019.03.014

Synthesis of a novel pyrene derived perimidine and exploration of its aggregation induced emission, aqueous copper ion sensing, effective antioxidant and BSA interaction properties

Nilanjan Chakraborty[a,b], Senjuti Banik[b], Arijit Chakraborty[c*], Swapan Kumar Bhattacharya[b], Suman Das[b*]

[a]Department of Chemistry, Maulana Azad College 8, Rafi Ahmed Kidwai Road, Kolkata 700 013, India.

[b]Department of Chemistry, Jadavpur University, Kolkata 700 032, India.

[c]Department of Chemistry, Acharya B N Seal College, Cooch Behar, West Bengal 730 161, India.

*Corresponding Authors

To whom all correspondence should be addressed.

Suman Das

Department of Chemistry

Jadavpur University

Raja S. C. Mullick Road, Jadavpur

Kolkata 700 032; India

Tel.: +91 94 3437 3164, +91033 2457 2349

Fax: +91 33 2414 6266

E-mail: sumandas10@yahoo.com

Abstract: A new pyrene derived dihydroperimidine [2-(pyren-1-yl)-2,3-dihydro-1*H*-perimidine (**1**)] was synthesized and characterized by ^{1}H-NMR, ^{13}C-NMR, HRMS spectroscopic techniques. The perimidine **1** was found to be a very interesting AIE luminogen with highest emission at 4:1 water-acetonitrile mixture. Compound **1** is a selective naked eye colorimetric sensor for aqueous Cu^{2+} (colorless sensor turned brownish yellow upon contact with Cu^{2+} ion) and gives turn off fluorescence responses in excited state spectroscopy with a limit of detection in the nanomolar range. Further it is an effective antioxidant which has been validated via 2,2- diphenyl-1-picrylhydrazyl assay and cyclic voltammetric studies in comparison to a well-known antioxidant L-ascorbic acid. To say vehemently antioxidant **1** has proven itself 5.9 times better than L-ascorbic acid. The perimidine **1** manifested interaction with protein bovine serum albumin via quenching of its own intrinsic emission intensity in Tris-HCl buffer.

Key words: Pyrene based perimidine; Aggregation Induced Emission; Colorimetric and turn off copper sensor; Strong antioxidant; Interaction with bovine serum albumin

1. Introduction

In the last few years scientists have been focusing on the development of organic luminogens exhibiting feeble emission in dilute solution whereas enhanced emission upon aggregation, i.e., aggregation induced emission (AIE) phenomenon/aggregation induced emission enhancement (AIEE) [1-10]. Fluorophores with AIE properties have found their utilities in optoelectronic and sensory systems. The AIE exhibitors are promising materials for OLEDs [11] and further fabrication of these OLEDs to electroluminescent devices [12]. They have also been accomplished as selective chemosensors, bioprobes [13-15], non-linear optical materials [16, 17], logic system modulators [18] and many others.

Designing and development of chemosensors for cations and anions those are environmentally and biologically important have become an intriguing job for the present day chemist [19-26]. Cu^{2+} demands its importance in the list amidst the biologically important metal cations being the third largest abundant transition metal ions in human body. It maintains homeostasis in human body which is exigent for the metabolism and development [27-29]. Its pivotal role is used by many proteins in electron transport as cofactors such as superoxide dismutase, cytochrome oxidase and tyrosinase [30, 31]. It catalyses redox reactions in cells, and it acts both as antioxidant, helping in reducing free radicals [32-34] as well as pro oxidant. Excessive presence of copper causes toxicity due to its catalytic activity in generation of free radicals which leads to various neurodegenerative and other diseases. Diseases like Wilson disease, Alzheimer's disease, Indian childhood cirrhosis, Menkes, and prions disease [35-38] owe their occurrence due to cellular toxicity of copper. Chronic long time exposure may result in impairment of liver and kidney. Even toxicity of Copper has its adverse effect in aquatic biota mostly in fishes and molluscs [39] among many one of which is impairment of olfactory responses in Coho salmon [40]. Due to extensive use of copper and its salts in daily lives via water pipes, utensils, wirings, medicines, fungicides etc. contamination is very likely.

Environment Protection Agency (EPA) has limited its amount to 1.3 ppm [41] which is roughly 20 μM in drinking water. Thus its detection and estimation is a high substantial matter.

The reactive oxygen species (ROS) and / reactive nitrogen species (RNS) are the oxygen or nitrogen centered free radicals such as superoxide, hydroxyl and nitric oxide. They are generated in biological system from both exogenous and endogenous origin [42-44]. These free radicals have deleterious role in physiology of organisms leading to various life threatening diseases. Excess exposure to free radicals can cause irreversible damages despite body's own regulatory mechanism causing damage to proteins, lipids and nucleic acids. These damages lead to life limiting chronic diseases like cancer, cardiovascular diseases, liver injury, diabetes, neurodegenerative disorders, rheumatism, atherosclerosis, ageing and autoimmune disorders [45-48]. Antioxidants are free radical scavengers making them nonreactive have found their application in therapeutic application for free radical induced diseases [49]. Besides naturally occurring antioxidants like ascorbic acid, carotenoids synthetic organic antioxidants are also appealing in the field. The efficiency of the antioxidants can be estimated by radical scavenging capacity (RSC) by spectrophotometric methods using a well-known 2,2-diphenyl-1-picrylhydrazyl (DPPH) assay [50] and cyclic voltammetry.

Binding of various drugs to plasma proteins like serum albumin is a predominant affair for biomedical and pharmaceutical studies related to drug discovery. Bovine serum albumin (BSA here after) is one of most studied proteins because of its repeating pattern of disulphide linkage and its structural homology (about 76%) with human serum albumin [51]. BSA is composed of 583 amino acid residues in a single polypeptide chain with intrinsic fluorescence due to two tryptophan (Trp here after) residues Trp 134 and Trp 212 [52]. Fluorescence method can be considered as a tool to study its binding properties.

Pyrene based motifs are reported to be good AIE luminogens [9, 53] and 2,3-dihydroperimidines have been known for their wide range industrial application in ion sensing

and biological activities [54, 55]. In the present piece of work we have synthesized a novel 2,3-dihydroperimidine derivative (**1**) derived from pyrene-1-carboxaldehyde and 1,8-diaminonaphthalene; the synthesized compound is an AIE active luminogen, aqueous Cu^{2+} ion sensor, an efficient antioxidant and a binder to plasma protein BSA.

2. Experimental section

2.1. Materials and instrumentation

All solvents of analytical grade were purchased from Merck, India and reagents were obtained from Spectrochem, India and used without further purification. Bovine serum albumin (BSA) was obtained from Sigma Aldrich Corporation. Tris base was obtained from Sigma Aldrich and to the 50 mM solution of the tris base appropriate dilution of HCl was added drop wise to make tris-HCl buffer of pH=7.4 and the buffer solution was filtered through milipore filter of 0.45 μm pore size before study. Both ^{1}H and ^{13}C NMR spectra were recorded using a Bruker 300 MHz (Bruker AVANCE 300) spectrometer and were recorded at an ambient temperature. ESI-MS was recorded using Q-tof-micro quadrupole mass spectrometer. UV-vis spectra of receptors were recorded in HPLC grade acetonitrile on a Perkin-Elmer UV/VIS spectrometer (Model: Lambda 25). Fluorescence spectra were generated on a Perkin Elmer Fluorescence spectrometer (Model: LS 55). The melting points were determined on a LabX, India Digital Melting Point apparatus and are uncorrected. All weighing were done in Mettler Toledo Analytical Balance Band (Model: MS 2045).

*2.2. Synthesis of 2-(pyren-1-yl)-2,3-dihydro-1H-perimidine (**1**)*

To 5 mL ethanolic solution of 1-Pyrenecarboxaldehyde (230 mg, 1.0 mmol), 1,8-diaminonaphthalene (158 mg, 1.0 mmol) and two drops of glacial acetic acid were added. The reaction mixture was refluxed for 2.5 hours. The resulting precipitate was collected by filtration. The filtered solid was washed with ethanol, water and dried to obtain pure rosy brown powdery solid. Yield: 363 mg (98%); M.P. 220 °C. The obtained compound has ^{1}H NMR (300

MHz, DMSO-d_6): δ 8.95 (d, *J* = 9.3 Hz, 1H), 8.38 (d, *J* = 5.3 Hz, 2H), 8.31 (d, *J* = 7.6 Hz, 2H), 8.21 (d, *J* = 8.5 Hz, 3H), 8.08 (t, *J* = 7.6 Hz, 3H), 7.20 (t, *J* = 7.8 Hz, 2H), 7.06 (d, *J* = 8.0 Hz, 2H), 7.00 (s, 2H), 6.55 (d, *J* = 7.2 Hz, 2H), 6.30 (s, 1H) (Supplementary materials, Fig. S1). ^{13}C NMR (75 MHz, DMSO-d_6): δ 144.20, 135.08, 134.37, 131.63, 131.26, 130.73, 129.53, 128.20, 127.86, 127.61, 127.36, 126.80, 125.85, 125.76, 125.19, 125.05, 124.77, 124.47, 115.03, 113.12, 105.03, 66.13 (Supplementary materials, Fig. S2). TOF MS-ES$^+$ spectral study have shown an intense molecular ion peak at 371.18 [**1**+H] (Supplementary materials, S3).

2.3. Spectrophotometric and spectrofluorimetric studies

For the exhibition of AIE features absorption and emission spectra of the compound **1** (10μM) were taken various fraction of water-acetonitrile mixture. The excitation and emission slits were kept at 10 nm and 7 nm respectively.

To investigate sensor properties 10 mM stock solution of the sensor **1** was prepared in $(CH_3)_2SO_3$. The stock solutions of the metal salts of 10mM concentration were prepared in water. For UV-vis analysis 2 μL of the stock solution of the receptor was added to 2 mL of acetonitrile in the cuvette to make the receptor solution of 10 μM concentrations. To the receptor solution of **1** (10 μM) in acetonitrile 7.44 equivalent aqueous solution of each cation was added.

Exploration of sensor properties through emission studies the same stock used for absorption studies was utilized. To the 10 μM solution of the compound **1** in acetonitrile 3 equivalent aqueous solution of each cation was added. All spectra were taken at ambient temperature. The light pathlength of fluorescence cuvette was 1cm. The excitation and emission slit of the spectrofluorimeter were kept at 10 nm and 7 nm respectively.

Inspection for protein-ligand interaction was performed in Tris-HCl solution. Known extinction coefficient value of 43824 $M^{-1}cm^{-1}$ at 280 nm was used to calculate the concentration of BSA solution. For absorption studies 10 μM of ligand **1** was titrated with BSA solution up

to 0.51µM. In fluorescence experiments albumin BSA (0.32 µM) was titrated with ligand **1** (up to 99 µM) and reversibly ligand **1** (10 µM) was titrated with protein BSA (0.76 µM).

All spectra were taken at ambient temperature. The light path length of both the absorbance and fluorescence cuvette was 1cm. The excitation and emission slits of the spectrofluorimeter were kept at 10 nm and 7 nm respectively for every investigation.

2.4. Fluorescence lifetime studies

Time correlated single photon counting (TCSPC) measurements were carried out for the properties like AIE (in acetonitrile-water fractions), Cu^{2+} sensation (in acetonitrile) and for BSA interaction in (Tris-HCl buffer). For all the studies the photo-excitation was made with a picosecond diode laser (IBH Nanoled 07) in an IBH fluorocube apparatus. The fluorescence decay data were collected on a Hamamatsu MCP photomultiplier (R3809) and were analyzed by using IBH DAS6 software using the following equation [56]:

$$F(t) = \sum \alpha_i e\left(\frac{t}{\tau}\right) ----(1)$$

Where, α_i is the i-th pre-exponential factor and τ is the decay time. The decay time is the life time of the excited species. The photoexcitation was made at 330nm for both AIE and Cu^{2+} sensing studies and the monitoring wavelengths were at 471nm and 398nm respectively. For BSA interaction studies the excitation was made at 370nm and monitored at 474nm.

2.5. Fluorescence quantum yield measurement

The fluorescence quantum yield [57, 58] of the fluorophore **1** (with reference to 1-pyrene-carboxaldehyde) in methanol was determined using the following equation:

$$\frac{\phi_s}{\phi_r} = \frac{I_s}{I_r} \times \frac{A_r}{A_s} \times \frac{\eta_s^2}{\eta_r^2} ----(2)$$

In eqn. 2 ϕ_s is the quantum yield of the sample whereas ϕ_r is the quantum yield of the reference used. A_r is the absorption maxima and I_r is the integrated peak area at the maximum intensity of the reference. A_s is the absorption maxima of the sample and I_s is the integrated peak area at

the maximum intensity of the sample. η_r and η_s are the refractive indices of the reference medium and the sample medium respectively.

2.6. Determination of binding constant

The spectrophotometric titration data was used to construct Benesi-Hildebrand [59] plot to determine binding constant from the following equation:

$$\frac{\Delta A_{\max}}{A} = 1 + \frac{1}{K_{BH}[C]} ----(3)$$

$\Delta A = |A_x - A_0|$ and $\Delta A_{max} = |A_\infty - A_0|$. A_0, A_x and A_∞ are the absorbance of compound **1** in absence of F^-, at an intermediate cation concentration and at a concentration of complete saturation with Cu^{2+} respectively. K_{BH} represents the binding constant of **1**-Cu^{2+} complexation, [*C*] is the concentration of the variant (here in Cu^{2+}). Plot was made with $\Delta A_{max}/\Delta A$ as a function of 1/[*C*]. The binding constants can be obtained from the slope.

The binding constant for BSA protein binding studies was obtained from emission titration profile utilizing Benesi-Hildebrand equation:

$$\frac{\Delta I_{\max}}{I} = 1 + \frac{1}{K_{BH}[C]} ----(4)$$

$\Delta I = |I_x - I_0|$ and $\Delta I_{max} = |I_\infty - I_0|$. I_0, I_x and I_∞ are the emission intensities of BSA/**1** in absence of compound **1**/BSA, at an intermediate protein/ligand concentration and at a concentration of complete saturation with ligand **1**/protein BSA respectively. K_{BH} represents the binding constant of the complex formation between compounds **1** and BSA and [*C*] is the concentration of the variant.

The binding stoichiometry of the **1**-Cu^{2+} complex was determined by continuous variation method of Jobs [60], from absorption profile. The relative change of absorbance (ΔA) was plotted as a function of increasing mole fraction of Cu^{2+} ions. ΔA is the difference of absorbance between bound receptor and free receptor at 341 nm. The total molar concentration of the sensor **1** and Cu^{2+} was kept at 50 μM.

2.7. pH dependence of absorption and emission spectra of receptor 1.

To investigate into pH dependence of sensor **1**, 10 μM of the sensor **1** in buffer solutions of various pHs were examined. The changes in wavelength of the emission maxima and emission intensities were noted. The buffers were: pH 1-2, HCl/KCl; pH 3-7, citric acid/Na_2HPO_4; pH 8, $NaH_2PO_4/NaHPO_4$; pH 9, $Na_2B_4O_7/H_3BO_3$; pH 10, $Na_2CO_3/NaHCO_3$.

2.8. Preparation of samples to access antioxidant activity in 2,2-diphenylpicrylhydrazyl (DPPH) assay

0.01 M methanolic solution of compound **1** was diluted to 1/2, 1/4, 1/8, 1/6, 1/32. 10 μL of 0.01 M prepared solution of 2,2-diphenylpicrylhydrazyl (DPPH), a commonly used radical scavenger sample solution was added to seven vials. Out of seven vials 10 μL each serially diluted solutions of compound **1** were mixed with six vials. 10μL of methanol was added to the seventh one which was studied for blank. All the vials were diluted to 2mL with methanol and incubated at room temperature in dark for 30 minutes. Similar procedure was tried with similar concentrations of L-ascorbic acid. The absorbance at 517 nm of the incubated solutions and the blank (without sample) were recorded. RSC (Radical scavenging activity) of the sample and the standard (here L-ascorbic acid) was plotted as a function of concentration. RSC was calculated using the following equation:

$$RSC = 100 \times \frac{A_{blank} - A_{sample}}{A_{blank}} ----(5)$$

A_{blank} represents the absorbance of the DPPH solution in methanol; A_{sample} represents the same in presence of antioxidants.

2.9. Antioxidant study by cyclic voltammetric (CV) studies

10mM of compound **1** and L-ascorbic acid were made propylene carbonate using tetrabutylammonium perchlorate as a supporting electrolyte. Calomel electrode was used as a

reference electrode whereas platinum wire and platinum foil were used as working and counter electrode respectively. The scanning range was -1 volt to +1 volt with a scan rate of 0.05 volt.

2.10. Dynamic Light Scattering (DLS) measurements

Mean hydrodynamic diameter of the aggregates of **1** in CH_3CN-water mixtures was determined by DLS using a fixed angle apparatus (Model DLS-nano ZS90, Zetasizer Nanoseries, Malvern Instruments). The scattering intensity was measured at an angle of 175º.

3. Results and discussion

3.1. Synthesis and Characterization

1,8-diamino naphthalene reacts with aldehydes/ketones in alcohol or benzenes to yield 2,3-dihydroperimidines [61]. Employing pyrene-1-carboxaldehyde as an aldehyde and keeping ethanol as solvent we have derived a novel 2,3-dihydroperimidine derivative (**1**) from 1,8-diaminonaphthalene with high yield of 98% (Scheme 1). The synthesized compound was characterized with ^{1}H-NMR, ^{13}C-NMR and HRMS spectroscopy. Owing to poor solubility of

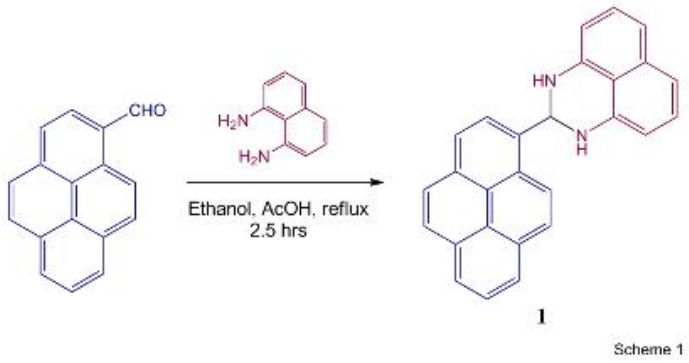

Scheme 1. Synthesis of chemosensor **1**

perimidine **1** in water and good solubility in organic solvents UV-vis spectrum of **1** was obtained in acetonitrile. The absorption spectra for **1** appeared with a prominent band at 341nm with a shoulder at 325nm and a band at 274nm with a shoulder at 264nm. The emission spectrum of **1** exhibited maximum intensity peak at 398nm with a shoulder peaks at 380 and 415nm when excited at 341nm. The emission band at 415 nm falls in the range of monomeric emission of pyrene.

*3.2.1. AIE features of the luminogen **1***

Investigation of AIE feature of the perimidine derived from pyrene was done in CH_3CN mixture by varying volume percentage of H_2O. Acetonitrile was used as good solvent while water as a poor one while inspecting the AIE characteristics of the compound **1**. The concentration of compound **1** in various water fractions (0-100%) CH_3CN-H_2O mixture was kept at 10μM for both absorption and emission studies. The aggregation was noted at higher water fractions in the CH_3CN-H_2O mixture. The luminogen **1** exhibited its characteristic absorption spectrum with peaks at 341nm, 325nm, 274 nm and at 264nm in pure acetonitrile. The increase in water fraction up to 70% doesn't seem to have effect in the absorption spectrum. At the higher water content in the CH_3CN-H_2O mixture (80%-100%) the peaks got broadened with decrease in intensity. A red shift of 10nm was noticed at 90%-100% water percentage. The fluorophore **1** when excited at 341 nm in acetonitrile exhibited an emission maximum at 398nm with a shoulder peaks at 380nm and 415nm. When water fraction was increased there was gradual increase in emission intensity and prominence of the shoulder peaks. A gradual red shift of the peak at 415 nm with increase in water percentage was noted up to 471 nm (a shift of 56 nm) at maximum emission. The maximum emission for aggregation was at 80% volume percentage of water. The intensity of the shifted peak increased gradually till 70% water fraction with a sudden hike at 80% water fraction (7.1 fold and 1.36 fold more with respect to pure acetonitrile and 70% water fraction respectively). The increase in water content witnessed the generation of new peak around 418-420 nm. At 80% water in CH_3CN-H_2O mixture when emission induced by aggregation was maximum the spectra was characterized by four distinct peaks at 378 nm (10.3 fold more intense than in CH_3CN), 398 nm (6.55 fold more intense than in CH_3CN), 419 nm and 471 nm (7.1 fold more intense than in CH_3CN). When the volume of water increased to 90% the intensity drops down by 2.2 fold with respect to intensity at 80% water fraction with a red shift to 476nm. In 100% water a flat peak (485 nm-522 nm) with much decreased intensity was observed. The absorption and emission spectra of the compound **1** in various water fractions in CH_3CN-H_2O mixture has been depicted in Fig. 1A and Fig. 1B.

The aggregation of the compound **1** in higher water fractions of CH_3CN-H_2O mixture was also evident in naked eyes (Fig. 1C) and AIE was evident under UV light illumination at 366nm (Fig.1D).

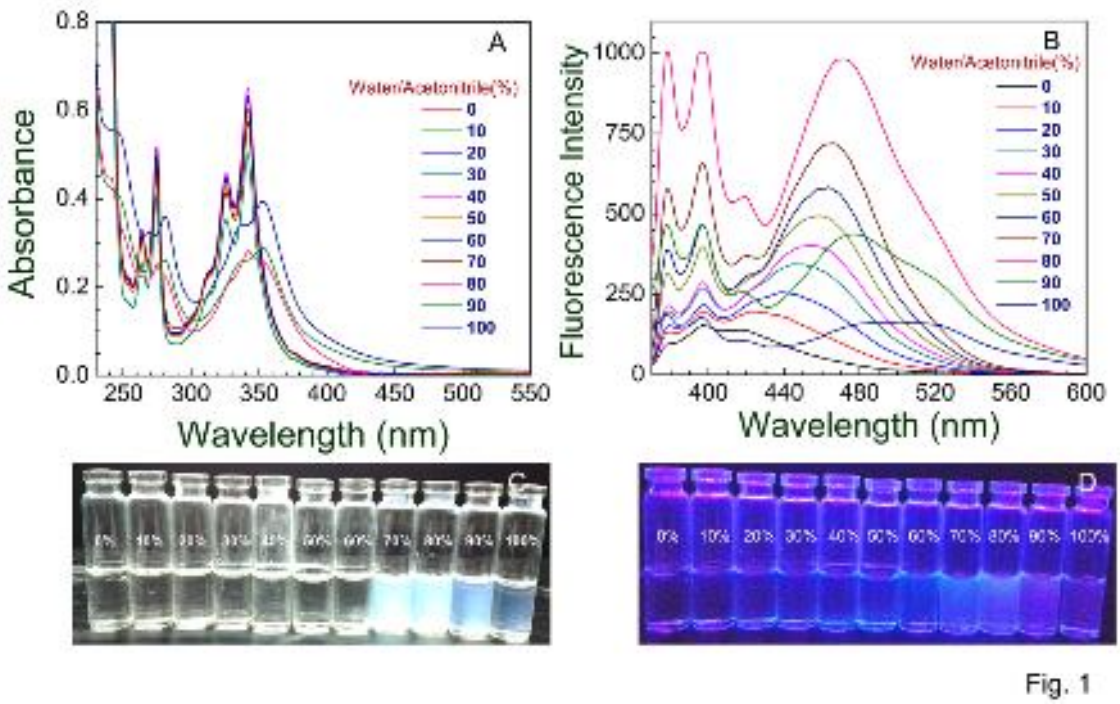

Fig. 1

Fig. 1. A) Absorption spectrum of **1** (10 μM) in various percentage of water in acetonitrile. B) Emission spectrum of **1** (10 μM) in various percentage of water in acetonitrile. C) Naked eye observation of **1** (100 μM) in various percentage of water in acetonitrile. D) Observation of **1** (100 μM) in various percentage of water in acetonitrile under UV illumination at 366nm.

In addendum time resolved fluorescence technique was employed to study the AIE feature of the luminophore **1**. A lifetime study have been represented by decay profiles of intensity (log scale) versus time (ns) and is presented in the Fig. 2, the corresponding data are tabulated in Table 1. In acetonitrile the multi-exponential decay of the luminogen **1** has been ascribed to three different species. The longer lifetime τ_3 corresponds to the pyrene emission, as obvious from the notion of delayed fluorescence, whereas the moderate lifetime τ_1 is the signature of the perimidine part. The ultrafast lifetime (τ_2) is probably the outcome of the charge-transfer species (perimidine to pyrene). At 80% water, however, the

amplitude of the charge-transfer species is found to significantly increase owing to the increasing polarity of the medium. Moreover, the component corresponding to the pyrene moiety exhibits a substantially augmented lifetime, which is the outcome of aggregation and/or excimer formation leading to stabilization. The average lifetime of compound **1** was calculated to be 0.76 ns in acetonitrile. The average life time (τ) of the hydrosol for 80% water fraction was found to be 0.34 ns. With the help of average lifetime and the quantum yield of the compound **1** in pure acetonitrile and 80% hydrosol the radiative rate constant (K_r) and the non radiative rate constants (K_{nr}) were calculated using the following equations:

$$\tau^{-1} = K_r + K_{nr} \quad ----(6)$$

$$K_r = \frac{\phi}{\tau} \quad ----(7)$$

The data related to lifetime studies have been depicted in the Table 1 where α value represents the relative amplitude of the decay components in the excited state where other terms have their usual meaning as mentioned in the text.

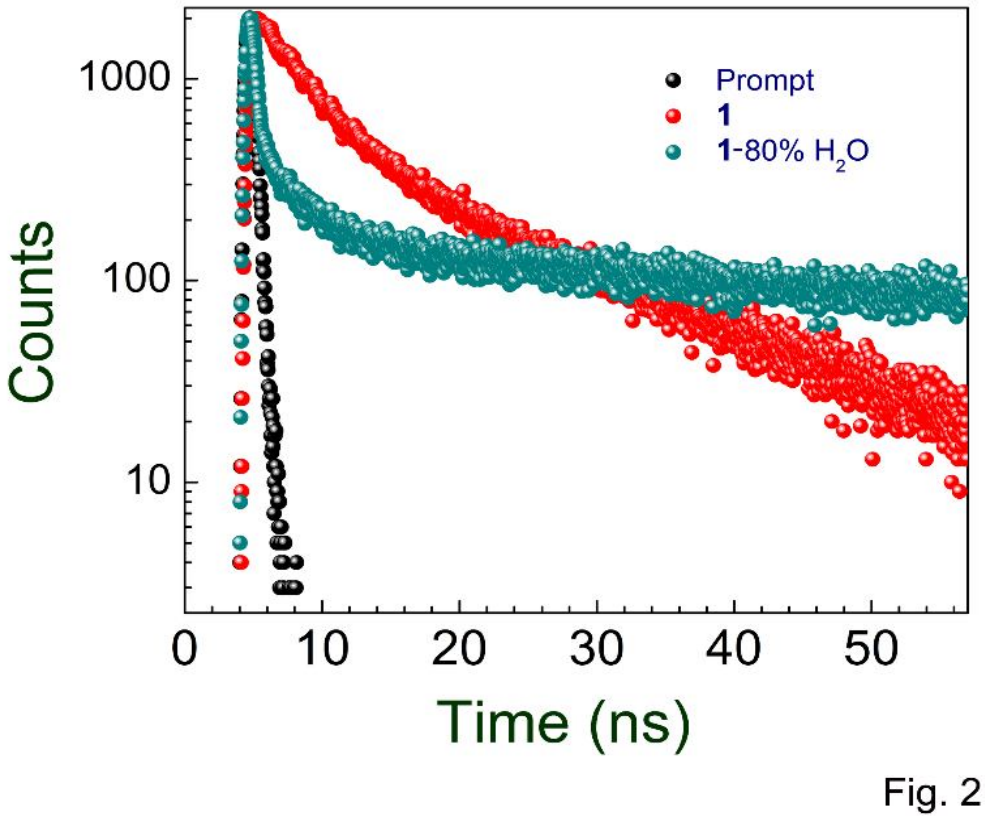

Fig. 2. Decay profile of **1** (10μM) in acetonitrile and in 80% of water in acetonitrile.

Table 1. Decay parameters of the time resolved study of AIE luminogen **1** in pure solvent and hydrosol form.

% of water in the CH_3CN medium	τ_1 (ns)	(α_1)	τ_2 (ns)	(α_2)	τ_3 (ns)	(α_3)	χ^2	Average life time (τ) of the fluorophore **1** (ns)	Quantum yield (ϕ)	Radiative rate constant (K_r) (ns^{-1})	Non radiative rate constants (K_{nr}) in ns^{-1}.
0	3.42	40.45	0.03	3.73	15.69	55.81	1.18	0.76	0. 026	0.034	1.282
8 0	3.10	6.84	0.05	13.35	83.23	79.81	1.07	0.34	0. 083	0.244	2.697

To verify further about the formation of aggregates the hydrosol having highest emission have been subjected to dynamic light scattering experiment (DLS). The results for DLS experiment have been depicted in Fig. 3, where the average size of the compound in 80% hydrosol has been found to be 260.55 nm. Moreover there was no precipitation of the hydrosol in the macroscopic level suggesting the formation of nanodimensional aggregates.

*3.2.2. Mechanistic explanation of AIE the luminogen **1***

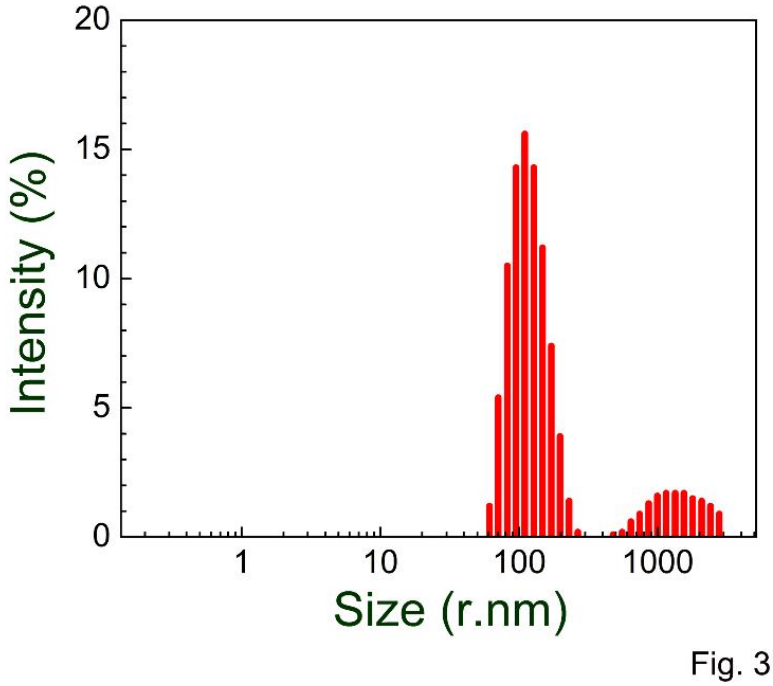

Fig. 3. DLS based particle size analysis of **1** in 80% of water in acetonitrile.

The origin of the AIE phenomena is probably due to restriction in intramolecular rotation (RIR) as discussed in earlier literatures [62]. The free rotation of the single bond between the perimidine part and pyrene part is responsible for the non radiative decay process thereby exhibiting weak emission. The emission spectra of **1** showed dual emission property at around 400 nm which is characteristics of pyrene monomeric emission (375-405 nm) and around ~460 nm, upon aggregation which may be attributed to pyrene-excimer formation. Upon aggregation there is restriction in free intramolecular rotation. The gradual enhancement in emission with red shift is assumed to be the cause of relatively planar geometry with suppression of twisted intramolecular charge transfer [63, 64] occurring due to cation-π interaction between pyrene and perimidine moieties. The blue shift and red shift in absorbance due to aggregation indicates *H*-type and *J*-type aggregation respectively [53]. In the absorption spectra of compound **1** in various water fraction exhibits a red shift in higher water volumes pointing at *J*-type

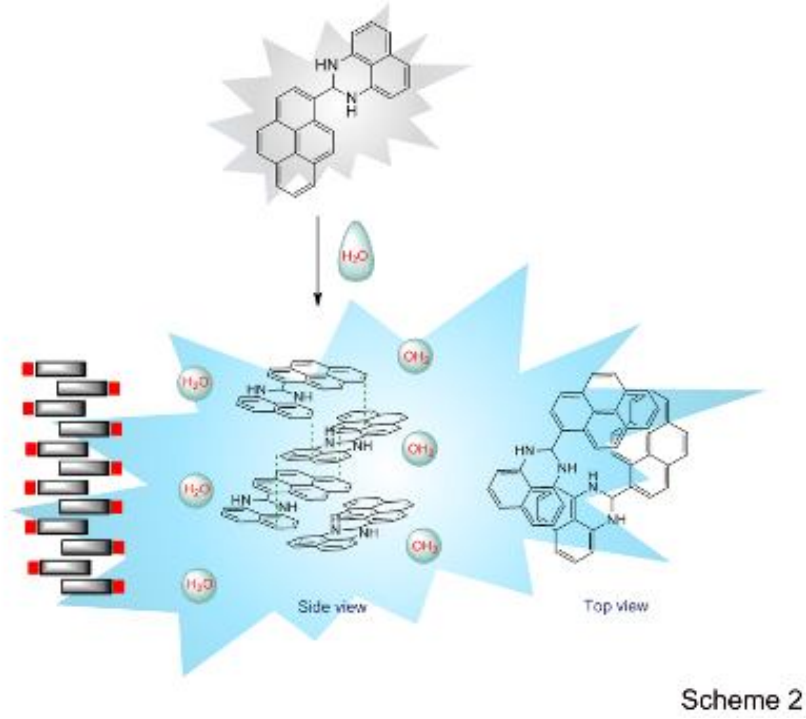

Scheme 2

Scheme 2. Probable ladder like *J*-type aggregation of AIE luminogen **1** in hydrosol (CH_3CN-H_2O).

aggregation. In Scheme 2 a probable ladder form of *J*-aggregate [65] formation has been

depicted considering the molecular structure of the luminogen **1**. Again from the determined radiative and non-radiative rate constants it is clear that in higher water fraction the non-radiative decay process is much hampered giving way to radiative one. The K_{nr} (non-radiative decay constant) value and K_r (radiative decay constant) value are both increasing on shifting from pure acetonitrile to 80% water fraction but K_r value is increasing 7.2 times whereas K_{nr} value is increasing only 2.1 times. The high jump in K_r value compared K_{nr} indicates at aggregation induced emission (AIE). On increasing water fraction beyond 80% the drop down in the fluorescence intensity is suggestive for formation of amorphous aggregates hampering crystallization process. The results obtained from absorption and emission spectra are clearly indicative for the AIE phenomenon.

3.3. Effect of Solvent polarity and viscosity

The effect of solvents of various polarities on absorption spectra and emission spectra were recorded for 10 μM of the perimidine **1**. There were no noticeable characteristic changes in absorption wavelength (bands I, II, III, IV) with variation of solvents (hexane, chloroform, ethanol, toluene, methanol, acetonitrile, dimethylformamide, dimethylsulfoxide) except in case of toluene where there was a red shift only in the high energy bands (band III and IV). The absorption wavelength changes with solvent variation have been depicted in Fig. S1 and tabulated in Table S1. In the emission spectrum the prominent peak of the fluorophore **1** around 398-399 nm and a broadened peak around 380 nm maintained their position with change in intensity on varying the solvent polarity. The peak at 415 nm for acetonitrile exhibited red shifts upon changing solvent environments. Large red shifts with increasing intensity were noticed for ethanol (448 nm), methanol (449 nm) and toluene (513 nm). For the solvent chloroform a new peak generated at 528 nm. The increase in intensity at region around 398-399 nm was examined. The peak in polar acetonitrile is less intense than feebly polar chloroform. Emission peak in toluene which is slightly less polar than methanol exhibited a

more intense peak than the later. The red shifted and less intense peak in case of protic solvents such as ethanol and methanol are probably due to nonradiative decay and stabilization resulting from H-bonding interaction with NH protons of **1**. Excepting the aforesaid exceptions the emission intensity increased with increase in dielectric constant of the solvents. The emission profile of **1** in various solvents has been depicted in Supplementary materials, Fig. S4 and tabulated in Table S1.

The emission profile of the compound **1** (10 μM) was also checked in solvents of varying viscosity. The solvent viscosity was varied by increasing percentage of highly viscous glycerol in methanol. The emission intensity got enhanced with increase in viscosity of the medium. In the highly viscous medium there was restriction in free rotation of the molecule. The operative RIR process in highly viscous environment hindered the non radiative decay process thereby enhancing the emission (Supplementary materials, Fig. S5).

3.4. Colorimetric and fluorescence sensing of cations

To acetonitrile solution of the sensor **1** (10 μM) 10 equivalent of the aqueous cations (Ag^{+}, Ba^{2+}, Ca^{2+}, Co^{2+}, Cr^{3+}, Cu^{2+}, Fe^{2+}, Hg^{2+}, K^{+}, Mg^{2+}, Na^{+}, Ni^{2+}, Pb^{2+} and Zn^{2+}) were added to note the colorimetric changes. Among all the cations the sensor in acetonitrile expressed its interaction by changing from colorless to brownish yellow in specific presence of Cu^{2+} ion (Fig. 4A). There were no notable changes were observed with other cations.

After naked eye responses to get further insight about the cationic interaction UV-vis absorption and spectrofluorimetric studies were performed. To 10μM solution of the sensor **1** in acetonitrile the absorption and emission behaviors were monitored upon addition of various cations viz. Ag^{+}, Ba^{2+}, Ca^{2+}, Co^{2+}, Cr^{3+}, Cu^{2+}, Fe^{2+}, Hg^{2+}, K^{+}, Mg^{2+}, Na^{+}, Ni^{2+}, Pb^{2+} and Zn^{2+}.

As mentioned earlier there were 4 absorption bands (two high energy bands and two low energy bands) of the free receptor at 341 nm (prominent peak), 32 5nm, 274 nm (prominent peak), and 264 nm. Upon interaction with cations the sensor **1** only responded to aqueous Cu^{2+}

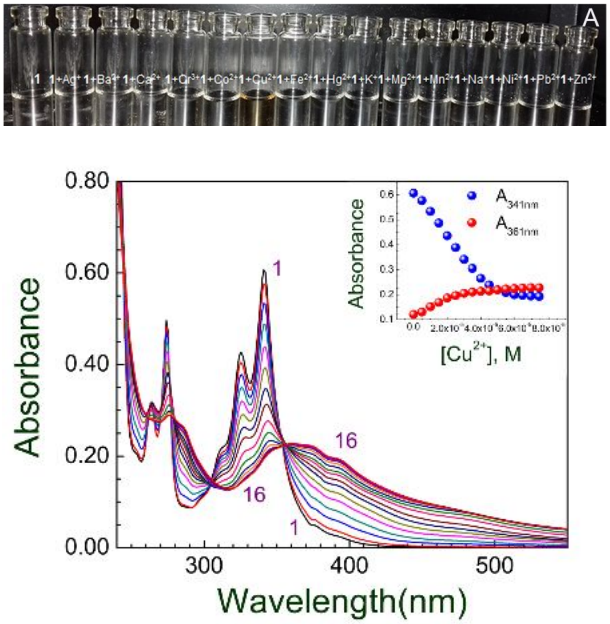

Fig. 5

Fi ...us

aq ...us

aq **Fig. 5.** Absorption spectrum of titration of sensor **1** (10μM) (curve 1) with aqueous Cu^{2+} (75μM) (curve 16) in acetonitrile; Inset: Plot of maximum absorption intensity at 341nm and 361nm versus Cu^{2+} concentration.

whereas the spectra exhibited minor changes in case of other aqueous cations (Fig. 4B). The absorption titration of the receptor **1** (10 μM) with Cu^{2+} ions up to saturation (75 μM) was performed. From the titration profile a ratiometric change was noticed where band of the free receptor at 341 nm, 325 nm, 274 nm and 264 nm gradually showed decrease in intensity while a new peak at 361 nm and 274 nm appeared with gradual increase in intensity with increasing analyte concentration (Fig. 5). There was a red shift of 20 nm of the high energy band at 341 nm **1** upon complexation with Cu^{2+}. The bathochromic shift is also indicative of stability after complex formation with Cu^{2+}. Clear isosbestic points appeared at 357nm and 304nm indicating the equilibrium of the complex formation (Scheme 3). The limit of detection (3σ/S) of the sensor **1** was determined from the calibration curve of ratiometric absorption (ratio of absorbance at 361 nm to 341 nm) as a function of concentration of Cu^{2+} (Supplementary materials, Fig. S6). The Limit of Detection (LOD) was determined to be 37.5nM which is much

below EPA's permissible limit which is ~20μM. The limit of detection has been compared with some other turn on/off Cu^{2+} sensor published in literature (Table 3) our sensor can be assigned to be a good aqueous Cu^{2+} ion detector.

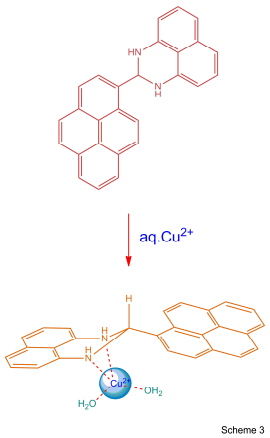

Scheme 3. Probable complex formation between compound **1** and Cu^{2+}.

The prominent emission band of sensor **1**was formed at 398 nm upon excitation at 341nm. At a time addition of the 5 equivalent of aqueous cations viz. Ag^{+}, Ba^{2+}, Ca^{2+}, Co^{2+}, Cr^{3+}, Cu^{2+}, Fe^{2+}, Hg^{2+}, K^{+}, Mg^{2+}, Na^{+}, Ni^{2+}, Pb^{2+} and Zn^{2+} to the 10μM solution of sensor **1** in acetonitrile

Table 2. Decay parameters of the time resolved study of sensor **1** and **1**+Cu^{2+} in acetonitrile.

Soluition	τ_1	(α_1)	τ_2	(α_2)	τ_3	(α_3)	χ^2	Average life time (τ) the phore **1** (ns)	Quantum yield	Radiative rate constant [1]	Non radiative rate constant (K_{nr}) in ns^{-1}.
1	3.42	0.030	0.03	0.290	15.69	0.009	1.18	0.76	0. 026	0.034	1.282
1+Cu^{2+}	4.14	0.005	15.52	0.011	0.11	0.221	1.15	1.41	0. 004	0.003	0.710

Table 3. A comparative study of limit of detection of sensor **1** with known Cu^{2+} ion sensors in literature.

Sensors	Limit of detection
3-Amino-7-hydroxy-2*H*-chromen-2-one, [64]	54.1 μM
1,2-diamino-anthraquinone, [65]	0.15 nM
Pyrene based benzothiazolen hydrazone, [66]	2.73 μM
1-(3,6'-Bis(diethylamino)-3-oxospiro[isoindoline-1,9'-Xanthen]-2-yl)urea, [67]	0.16 μM
1,5-dimethyl-2-phenyl-4-((pyren-1-ylmethylene)amino)-1H-pyrazol-3(2H)-one	2.5 μM

was monitored for further corroboration of the selectivity of the sensor through emission studies (Fig. 6). There was noticeable quenching of fluorescence for interaction with Cu^{2+}at 398nm. Quenching of intrinsic fluorescence intensity was also observed for Ni^{2+} and Cr^{3+}. The quenching efficiency of Cu^{2+} was 80% whereas for Cr^{3+} and Ni^{2+} it was 55% and 23% respectively. There were no significant changes in the emission spectrum of **1** upon interaction with other cations. It can be concluded that the turnoff emission on Cu^{2+} interaction is selective and extent of quenching due to Cr^{3+} or Ni^{2+} was not as extensive as Cu^{2+}. Sensor **1** (10μM) was titrated with Cu^{2+} until saturation up to 30μM (Fig. 7). With increase in Cu^{2+} concentration the peak at 398nm got quenched with a red shift of the peak at 415 nm to 425nm. Again the red shift in emission spectra is also suggestive for interaction of Cu^{2+} with NH protons. The Stern Volmer of quenching constant was obtained from relative intensity change versus concentration of quencher plot (Supplementary materials, Fig. S8) vide equn. 8. The quenching constant came out to be ~140000 M^{-1}.

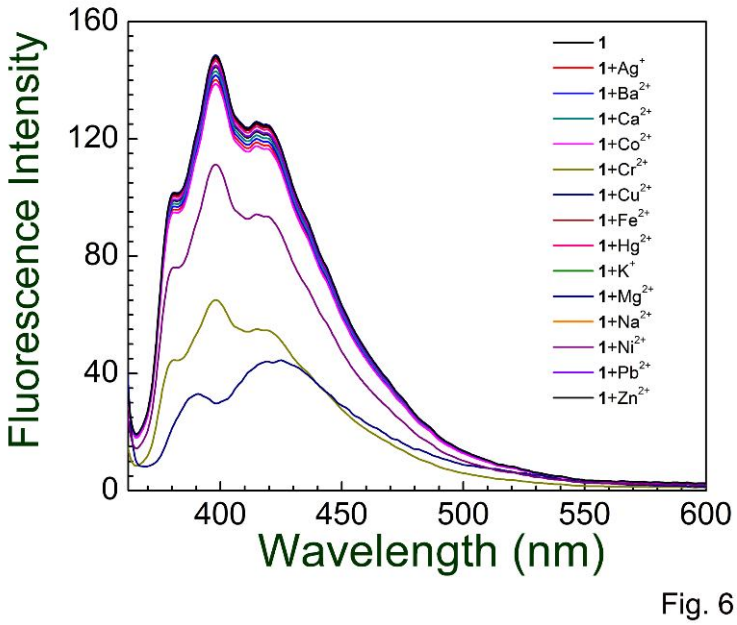

Fig. 6

Fig. 6. Emission spectrum of sensor **1** (10μM) with various aqueous cations (5 equivalent) in acetonitrile.

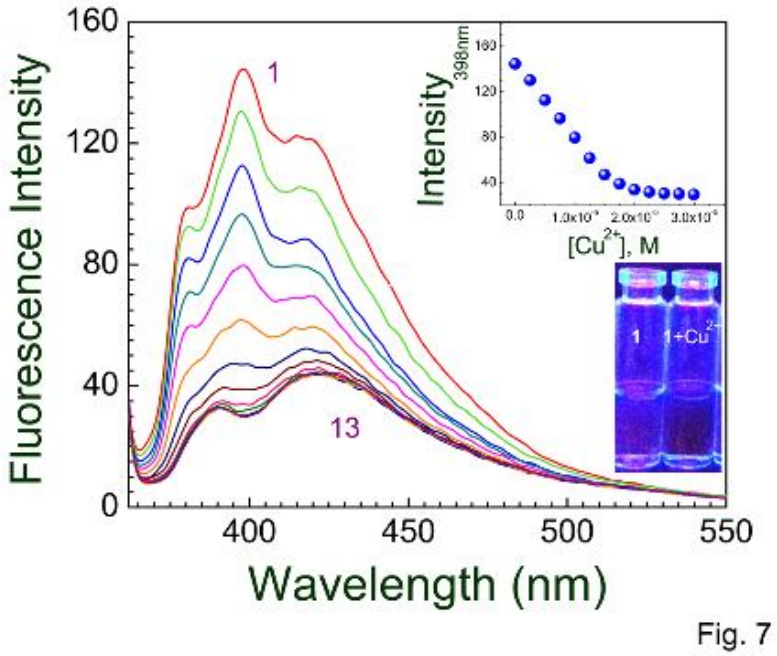

Fig. 7. Emission spectrum of titration of sensor **1** (10μM) (curve 1) with aqueous Cu^{2+} (30μM) (curve 13) in acetonitrile. Inset: Plot of maximum emission intensity at 398nm versus Cu^{2+} concentration (top); UV illuminated (at 366nm) view of free receptor **1** and Cu^{2+} quenched receptor **1** (bottom).

3.5. Fluorescence Lifetime studies of the cationic interaction

In emission life time studies representative decay profiles of intensity (log scale) versus time (ns) are plotted (Fig. 8). The lifetime data are presented in Table 2 where α values represent the relative amplitude of the decay components in the excited state. Average lifetime denotes the amount of time fluorophore (herein compound **1**) resides in the excited state during excitation. Decay profiles exhibiting multiexponential decay, signifies lifetime as a statistical average. In the present case the fluorophore **1** in both free form and bound form (binding with Cu^{2+}) exhibited a multiexponential decay profile in acetonitrile. The life time value of the free sensor **1** was increased from 0.76 ns to 1.41 ns upon interaction with Cu^{2+}. Increment in average lifetime of the fluorophore **1** indicates the stronger affinity of fluorophore **1** for Cu^{2+} in the experimental condition.

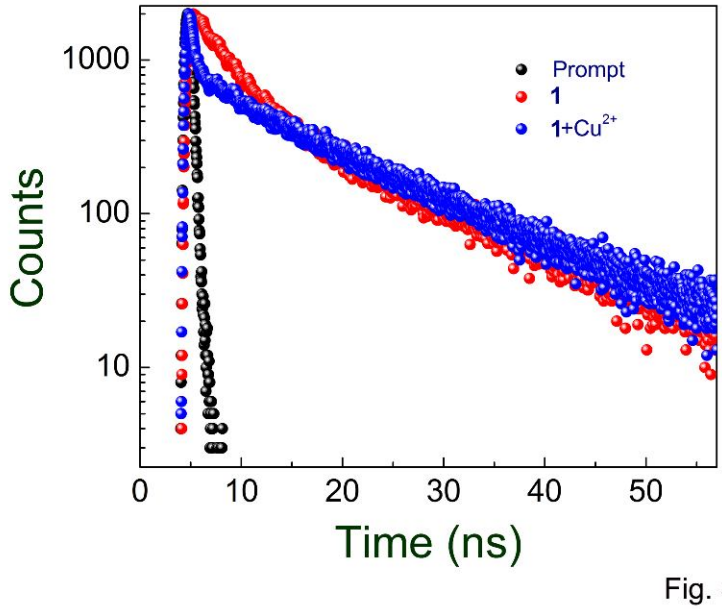

Fig. 8. Decay profile of sensor **1** and Cu^{2+} bound sensor **1** in acetonitrile.

3.6. Binding stoichiometry and binding constant

The method of continuous variation i.e., Jobs plot was employed to determine binding stoichiometry [60]. The Jobs plot was obtained from spectrophotometric titration profile. ΔA (the difference of absorbance between bound receptor and free receptor at 341 nm) was plotted as a function of increasing mole fraction of Cu^{2+} ions (Supplementary materials Fig. S7B). The total molar concentration of the sensor and Cu^{2+} was kept at 50 μM. The break point in the resulting plot corresponds to the mole fraction of cations in the cation:ligand complex. From our study, the inflection point was determined to be at 0.5 mole fraction of Cu^{2+}. The ratio of mole fraction at the point of inflection of Cu^{2+} to ligand **1** represent the binding stoichiometry of **1**-Cu^{2+}. Thus Cu^{2+} formed complex with **1** in 1:1 mode.

The binding constant (K_{BH}) of the receptor **1** with Cu^{2+} was evaluated by the method of Benesi-Hildebrand (B-H) [59] equation for 1:1 complex (discussed in experimental section). The binding constants can be obtained from the slope of the plot of $\Delta A_{max}/\Delta A$ as a function of

$1/[C]$ where $\Delta A = |A_x - A_0|$ and $\Delta A_{max} = |A_\infty - A_0|$. A_0, A_x and A_∞ are the absorbances of compound **1** in absence of Cu^{2+}, at an intermediate anion concentration and at a concentration of complete saturation with Cu^{2+} respectively (Supplementary materials Fig. S7A). The binding constant was found to be $9.877 \times 10^4\ M^{-1}$.

3.7. Competition experiment

To verify further the selectivity and specificity of sensor **1** for Cu^{2+} a competition experiment was performed with the help of emission studies. One time addition of 5 equivalents of each cation to 10 μM of sensor **1** was followed by at a time addition of 5 equivalents of Cu^{2+} ion (Fig. 9). The change in emission intensity at 398 nm was monitored to find the effect in quenching emission intensity sensor **1** by Cu^{2+} in presence of other coexisting ions. The quenching due to Cu^{2+} ion was maintained roughly, thus sensor **1** seems to be highly selective for Cu^{2+}.

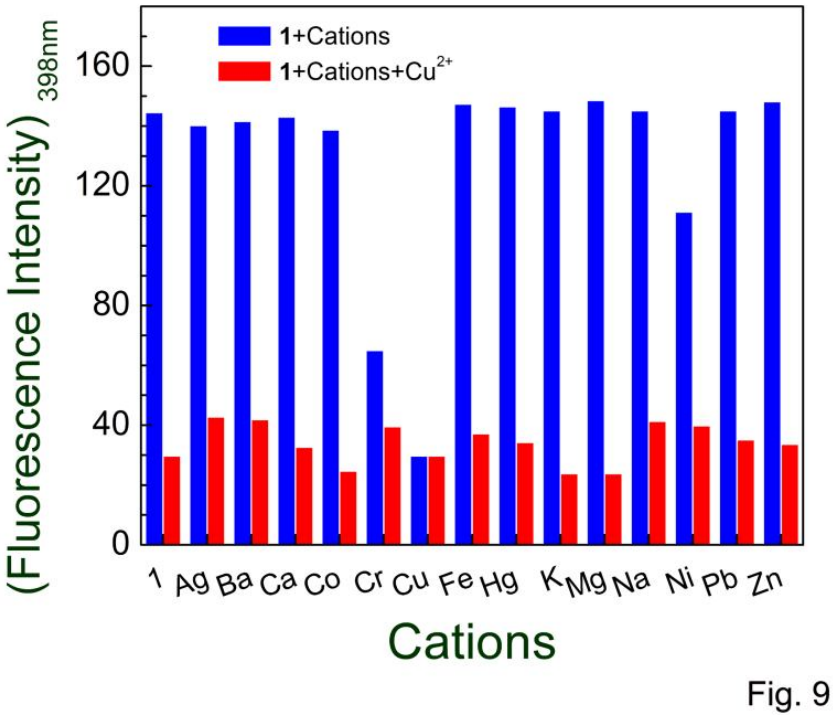

Fig. 9. Quenching of emission intensity of **1** by Cu^{2+} in presence of other competitive cations in acetonitrile at 398nm.

3.8. Detection of Cu^{2+} in water from real samples

The water samples were collected from various sources like river, pond and ground water sources. A known amount of Cu^{2+} was added to water samples and its recovery was noticed from ratio of absorbance intensities at 361nm to 341nm (Supplementary materials, Fig. S6). Experiment was repeated thrice for each real samples and the average of the results were taken. The detailed results have been depicted in Table 4. The good recovery results were obtained which points to its capability of detecting Cu^{2+} in real samples.

Table 4. Determination of Cu^{2+} from real samples.

Water samples	Sets	Cu^{2+} added (μg/mL)	Cu^{2+} found (μg/mL)	Average	Recovery %
River Water	1	2.09	1.75	1.92	91.86
	2	2.09	2.12		
	3	2.09	1.89		
Ground Water	1	2.19	2.14	2.04	93.15
	2	2.19	1.99		
	3	2.19	2.01		
Pond Water	1	2.89	2.53	2.69	93.08
	2	2.89	2.83		
	3	2.89	2.72		

*3.9. pH dependence of **1***

To check the effect of pH in the emission spectra of **1**, the 10μM solutions of the sensor in buffers of various pH (1-10) was excited at 341nm. There was very little change in wavelength with variation in pH a slight red shift was noticed at very low pH (1-2) (Supplementary materials, Fig. S9A). The emission intensity was low at pH 1 and sudden hike was notice at pH 2 again intensity drops at pH 3 and it remained very little fluctuating again a hike was noticed at high pH (9-10) (Supplementary materials, Fig. S9B). The stability in intensity value was more or less maintained at physiological pH. Thus it can be used effectively in physiological pH.

3.10. Antioxidant property

3.10.1. Antioxidant property from DDPH assay

Antioxidant property of the compound **1** was investigated from the ability of the antioxidant **1** to reduce 2,2-diphenylpicrylhydrazyl (DPPH) assay in methanol with the help of spectrophotometric studies [50]. 2,2-diphenylpicrylhydrazyl (DPPH) assay in methanol display a violet color due to unpaired electrons which upon reduction with electrons from antioxidant turns colorless. The antioxidant ability of the compound **1** was compared with well known antioxidant L-ascorbic acid (Fig. 10). The details of the experimental have been discussed earlier. The results of the activity have been depicted in Table and represented in Fig. where RSC (radical scavenging capacity) (eqn. 5) has been plotted as a function of

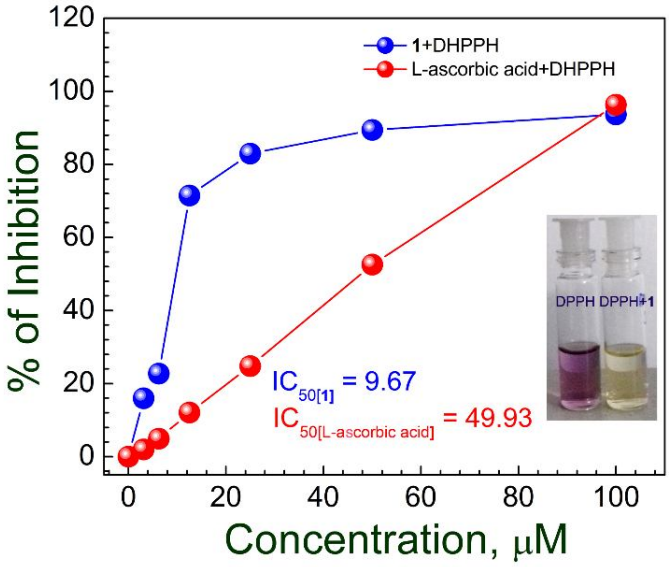

Fig. 10

Fig. 10. Percent inhibition of free radicals versus concentration of antioxidant (blue curve: antioxidant **1**, red curve: L-ascorbic acid) in DPPH assay. Inset: Colorimetric Change of DPPH assay in presence of radical scavenger **1** (100μM).

concentration of the antioxidants. IC_{50} is the concentration of the antioxidant at 50% RSC. From IC_{50} value the antioxidant **1** is found to be 5.9 times more capable than L-ascorbic acid.

*3.10.2. Antioxidant nature of **1** from Cyclic Voltammetric (CV) studies*

To further corroborate the better antioxidant nature of antioxidant **1** in comparison to L-ascorbic acid evident from DPPH assay cyclic votammetric (CV) experiments were performed. Since the synthesized compound is not enough soluble in water, the cyclic voltammetric study of the antioxidant property of the compound in comparison to that of L-ascorbic acid is carried out in propylene carbonate as solvent using tetra butyl ammonium perchlorate as supporting electrolyte. It is found that both the compound and the L-ascorbic acid exhibit three forward (oxidation) (x,y,z and a,b,c respectively) and three backward (reduction) peaks($x^{/}$,$y^{/}$,$z^{/}$ and $a^{/}$,$b^{/}$,$c^{/}$ respectively) indicating three step redox reactions for them (Fig. 11). Despite the first and second forward peaks for the compound become very broad due to merging, there corresponding backward peaks are prominent and occurred at lower potentials(-0.514V and -0.244V) than the potentials of similar backward peaks (-0.370V and -

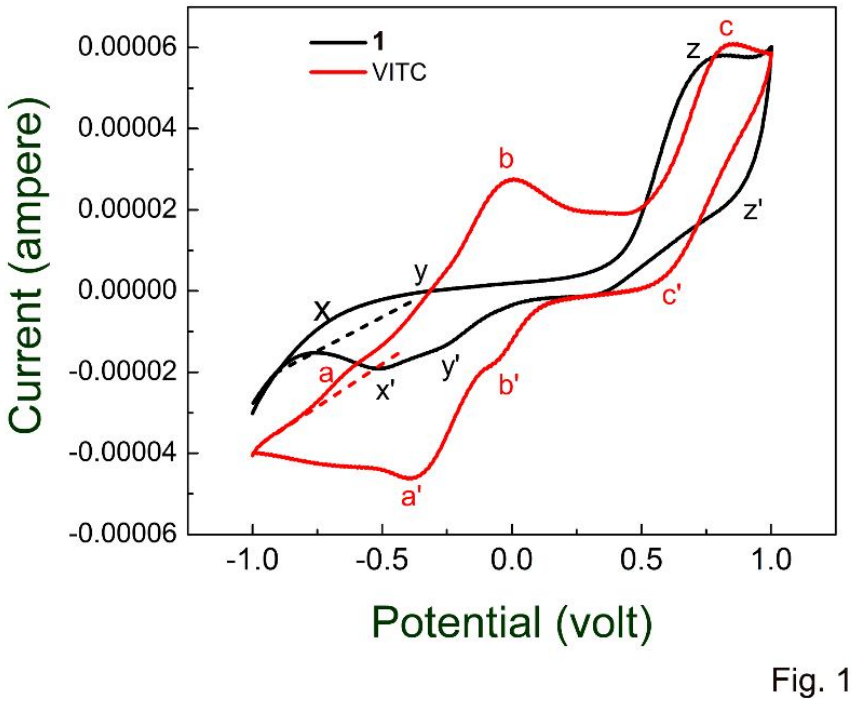

Fig. 11

Fig. 11. Cyclic-voltametric studies of antioxidants (black curve: antioxidant **1**, red curve: L-ascorbic acid).

0.058V) for ascorbic acid. Although the peak current values of the first two peaks of the

compound are small due to different orientation of the adsorbed compound through pi-electrons on the working electrode, its oxidation can be recognized by the positive current with respect to double layer current, long range of increased current and the corresponding reverse peaks for the reduction. The onset potential (-0.84V) and peak current for the first peak of the compound are respectively less and more than the corresponding potential (-0.78V) and current of the first peak of CV of ascorbic acid. Moreover the onset and peak potentials of the third and final peak of the compound (0.360V and 0.748V) are less than these of the final peak of ascorbic acid (0.480V and.0.850V). Again, the current value of the final peak of the former is comparable to that of the ascorbic acid. Thus it can be said that synthesized compound is more easily oxidized than ascorbic acid and so may act as a better oxidant than the latter.

3.11. Ligand-Protein interaction with BSA

UV-vis absorption method for studying spectral changes is an easy but potential way in the field of ligand–protein interaction. The compound **1** (10μM) has a characteristics absorption spectra in the range of 240-440nm with absorption maxima at 357nm with a shoulder peak at 339nm and 282nm in 2mL Tris-HCl buffer. The ligand **1** was titrated with increasing concentration of bovine serum albumin (BSA). There was a slight increase in absorption intensity upon addition of BSA with no shift in wavelength and saturation was obtained within 0.51μM of BSA concentration (Fig. 12A). A ligand-protein interaction was indicative from absorption studies. To further explore into the protein-ligand interaction the most potent and comprehensive fluorescence technique has been taken into consideration. In emission studies once ligand **1** was titrated with BSA (Fig. 12B) and at other time BSA was titrated with ligand **1** (Fig. 12C). The ligand **1** (10μM) has an emission maxima at 474nm when excited at 359nm

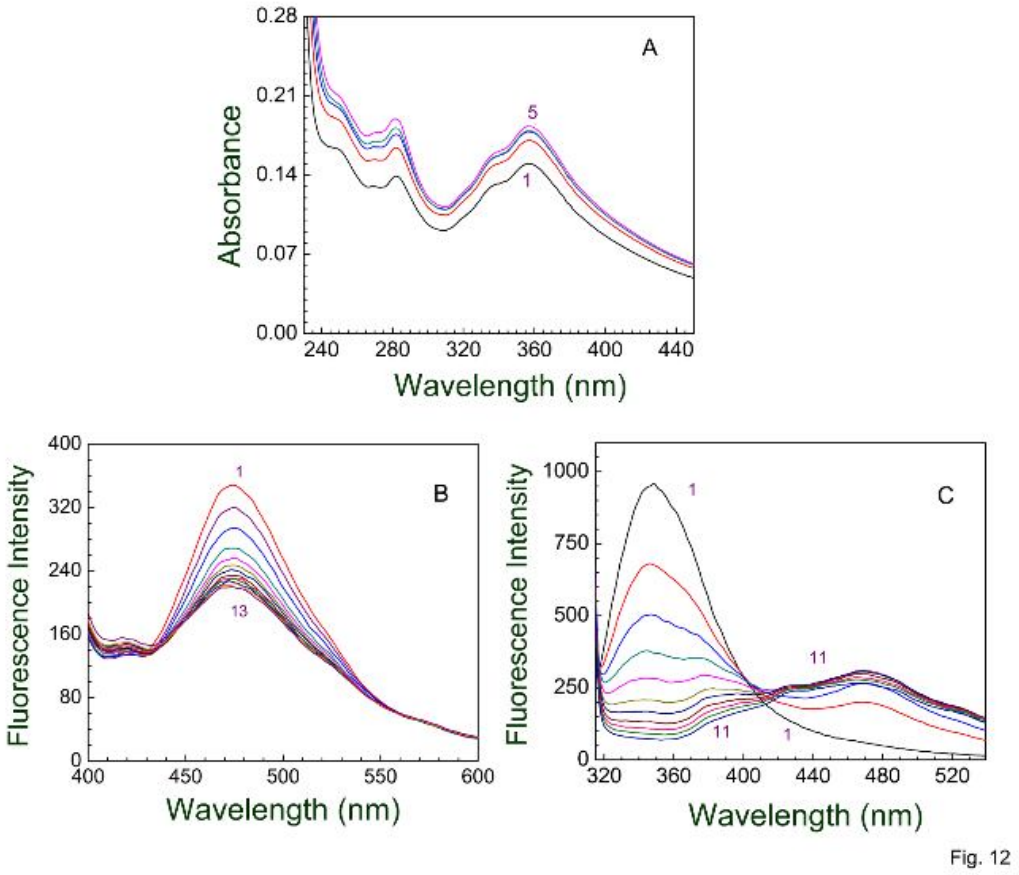

Fig. 12. A) Absorption spectrum of titration of sensor **1** (10μM) (curve 1) with BSA (0.51μM) (curve 5) in Tris-HCl. B) Emission spectrum of titration of sensor **1** (10μM) (curve 1) with BSA(0.76μM) (curve 13) in Tris-HCl. C) Emission spectrum of titration of BSA (0.32μM) (curve 1) with sensor **1** (98.76μM) (curve 11) in Tris-HCl.

in 2mL of Tris-HCl buffer (pH=7.4). It was titrated with incremental amount of BSA (0-0.76μM) till saturation. Upon BSA addition the intensity due to the ligand **1** got quenched. We know that BSA itself is sensitive towards fluorescence because of the Phenyl alanine (Phe), Tryptophan (Trp) and Tyrosine (Tyr) residues but the intrinsic fluorescence appears because of Trp residue [70]. When excited at 280nm, both Trp residues Trp 134 and Trp 212 and Tyr residues emit fluorescence whereas upon excitation near 295nm, fluorescence emission occurs due to Trp residue alone [71]. Trp 134 which resides in the hydrophilic region appears with an

emission maximum at higher wavelength whereas the Trp 212 is identified by a shorter wavelength maximum [72]. The intrinsic fluorescence due to Trp may alter upon ligand interaction with BSA. 0.32μM of BSA in Tris-HCl buffer was titrated with increasing concentration of ligand **1** 98.76μM with a gradual red shift from BSA peak at 348nm and a generation of a new emission peak at 465nm. The quenching of emission maximum with a red shift may be due to probable interactions such as excited state reactions, molecular rearrangements, energy transfer, ground state complexation or collision quenching etc. [73].

The results obtained from titration of **1** with BSA (Fig. 12) were used to determine the binding parameters. The binding constant of BSA to **1** can be obtained considering 1:1 complex formation using the equation of Benisi-Hildebrand (eqn. 3) discussed in experimental. K_{BH} representing the binding constant was found to be 5.32×10^6 M when BSA was used as variant (Supplementary materials, Fig. S11A). The extent of quenching of ligand intensity upon interaction with BSA was verified with Stern-Volmer quenching constant (K_{SV}) using the following equation:

$$\frac{I_0}{I} = 1 + K_{SV}[X] ----(8)$$

Where, I_0 and I are the fluorescence intensities of the free ligand and protein-ligand complex, [*X*] is the concentration of the quencher ion herein the protein and K_{SV} is the Stern–Volmer quenching constant. The accessibility of the bulky protein quencher to the ligand **1** is indicated from the K_{SV} values. K_{SV} is obtained from the slope the I_0/I versus [*X*] plot (Supplementary materials, Fig. S11C), which is imprecisely linear indicates the quenching to be static. The K_{SV} value obtained is 9.24×10^5 M^{-1} . The quenching efficiencies were calculated to be 59%. The binding parameters obtained after titrating BSA with ligand **1** were K_{BH}= 4.52×10^5M, K_{SV}=$9.96\times10^5M^{-1}$ and quenching efficiency is 86.67% (Supplementary materials, Fig. S11B and Fig. S11D). From the lifetime studies it was observed that average lifetime of **1**in Tris-HCl buffer is getting decreased from 0.27ns to 0.22ns.

4. Conclusion

It is concluded that we have derived a novel pyrene based perimidine which has multifunctional utility. Firstly, the compound **1** has been found to be a good AIE luminogen in CH_3CN-H_2O mixture forming nanodimensional aggregates. Secondly it has been a colorimetric and turnoff sensor for aqueous Cu^{2+} with specificity and selectivity. It binds with Cu^{2+} in 1:1 mode with binding constant of the order 10^4 M^{-1}. Sensor **1** can detect Cu^{2+} up to 37.5nM and is also applicable for detection of Cu^{2+} in real water samples. Thirdly, it has been an efficient antioxidant as it is 5.9 times more able than L-ascorbic acid in reducing DPPH assay. Lastly it can interact with BSA via fluorescence quenching. Therefore the novel pyrene based perimidine has been added as a new input in scientific research where it can further be used to develop OLEDs, determining Cu^{2+} in natural samples, as antioxidant to reactive oxygen species and in ligand-protein interaction and many others.

Conflict of Interest

The authors confirm that this article content has no conflict of interest.

Acknowledgment

AC gratefully acknowledges financial supports from Science and Engineering Research Board, DST, Government of India (SERB No.SR/FT/CS-116/2010) and SD gratefully acknowledges the financial assistance provided by the University Grant Commission (UGC), New Delhi, India [F. No. 43-243/2014 (SR), MRP-MAJORCHEM-2013-37991]. We also thank the Department of Chemistry, Maulana Azad College, Kolkata, West Bengal, India and Department of Chemistry, Jadavpur University, Kolkata, India. We acknowledge Dr. Aniruddha Ganguly of Jadavpur University for helping us with few explanations.

References:

[1]. J. Luo, Z. Xie, J.W.Y. Lam, L. Cheng, H. Chen, C. Qiu, H. S. Kwok, X. Zhan, Y. Liu, D. Zhu, B. Z. Tang, Aggregation-induced emission of 1-methyl-1,2,3,4,5-pentaphenylsilole Chem. Commun. 0 (2001)1740–1741

[2]. Z. Zhao, J.W.Y. Lam, B.Z. Tang, Tetraphenylethene: a versatile AIE building block for the construction of efficient luminescent materials for organic light-emitting diodes, J. Mater. Chem. 22 **(**2012) 23726–23740.

[3]. X. Du, J. Qi, Z. Zhang, D. Ma, Z.Y. Wang, Efficient Non-doped Near Infrared Organic Light-Emitting Devices Based on Fluorophores with Aggregation-Induced Emission Enhancement Chem. Mater. 24 (2012) 2178-2185.

[4]. J. Zhou, Z. Chang, Y. Jiang, B. He, M. Du, P. Lu, Y. Hong, H. S. Kwok, A. Qin, H. Qiu, Z. Zhao, B. Z. Tang, From tetraphenylethene to tetranaphthylethene: structural evolution in AIE luminogen continues Chem. Commun. 49 **(**2013) 2491–2493.

[5]. D. Ding, K. Li, B. Liu, B. Z. Tang, Bioprobes based on AIE fluorogens, Acc. Chem. Res. 46 **(**2013) 2441–2453.

[6]. T. Zhang, H. Ma, Y. Niu, W. Li, D. Wang, Q. Peng, Z. Shuai , W. Z. Liang, Spectroscopic Signature of the Aggregation-Induced Emission Phenomena Caused by Restricted Nonradiative Decay: A Theoretical Proposal, J. Phys. Chem. C. 119 (2015) 5040-5047.

[7]. H. Wang, E. Zhao, J.W.Y. Lam, B.Z. Tang, AIE luminogens: emission brightened by aggregation, Mater. Today 18 (2015) 365-377.

[8]. H. Ma, C. Qi, C. Cleng, Z. Yang, H. Cao, Z. Yang, J. Tong, X. Yag, Z. Lei. AIE-Active Tetrapphenylethylene Cross Linked N-Isopropylacrylamide Polymer: A Long Term Fluorescent Cellular Tracer, ACS Appl. Mater. Interfaces. 8 (2016) 8341-8348.

[9]. N. Chakraborty, A. Chakraborty, S. Das, A pyrene based fluorescent turn on chemosensor for detection of Cu^{2+} ions with antioxidant nature, J. Lumin. 199 (2018) 302-309.

[10]. N. Chakraborty, S. Bhuyia, A. Chakraborty, D. Mandal, S. Das, Synthesis and photophysical investigation of 2-hydroxyquinoline-3- carbaldehyde: AIEE phenomenon, fluoride optical sensing and BSA interaction study, J. Photochem. Photobiol. A 359 (2018) 53-63.

[11]. H. Y. Chen, W. Y. Lam, J. D. Luo, Y. L. Ho, Highly efficient light emitting diodes with a silole based compound, Appl. Phys. Lett. 81 (2002) 574.

[12]. Z. Zhao, S. Chen, J.W.Y. Lan, P. Lu, Y. Zhong, K. S. Wong, H. S. Kwok, B. J. Tang, Chem. Comm. 46 (2010) 2221-2223.

[13]. M. Shyamal, S. Maity, P. Mazumdar, G.P. Sahoo, R. Maity, A. Mishra, Synthesis of an efficient pyrene based AIE active functional material for selective sensing of 2,4,6-trinitrophenol, J. Photochem. Photobiol. A 342 (2017) 1-14.

[14]. Y. Hong, M. Haubler, J.W.Y. Lam, Z. Li, K.K. Sin, Y. Dong, H. Tong, J. Liu, A. Qin, R. Renneberg, B.Z. Tang, Label-Free Fluorescent Probing of G-Quadruplex Formation and Real-Time Monitoring of DNA Folding by a Quaternized Tetraphenylethene Salt with Aggregation-Induced Emission Characteristics, Chem. Eur. J. 14 (2008) 6428-6437.

[15]. H. Lu, B. Xu, Y. Dong, F. Chen, Y. Li, J. He, H. Li, W. Tian Novel fluorescent pH sensors and a biological probe based on anthracene derivatives with aggregation-induced emission characteristics, Langmuir 26 (2010) 6838-6844.

[16]. B. Xu, J. Zhang, H. Fang, S. Ma, Q. Chen, H. Sun, C. Im, W. Tian, Aggregation induced enhanced emission of conjugated dendrimers with a large intrinsic two-photon absorption cross-section, Polym. Chem. 5 (2014) 479-488.

[17]. Y. Duan, C. Ju, G. Yang, E. Fron, E. Countino-Gonzalez, S. Semin, C. Fan, R.S. Balok, J. Cremers, P. Tinnemans, Y. Feng, Y. Li, J. Hofkens, A.E. Rowan, T. Rasing, J. Xu, Aggregation Induced Enhancement of Linear and nonlinear optical emission from a hexaphenylene derivative, Adv. Funct. Mat. 26 (48) (2016) 8968-8977.

[18]. S. Pramanik, V. Bhalla, M. Kumar, Hexaphenylbenzene-based fluorescent aggregates for ratiometric detection of cyanide ions at nanomolar level: set-reset memorized sequential logic device, ACS Appl. Mater. Interfaces 6 (2014) 5930-5939.

[19]. D.A. Bushinsky, R.D. Monk, Electrolyte quintet: Calcium, Lancet. 352 (1998) 306-311.

[20]. W.J. Fawcett, E.J. Haxby, D.A. Male, Magnesium: physiology and pharmacology, Br. J. Anaesth. 83 (1999) 302-320.

[21]. A. Rastergar, M. Soleimani, Hypokalaemia and hyperkalaemia Postgrad. Med. J. 77 (2001) 759-764.

[22]. F. Sancenon, R. Martinez-Manez, J. Soto, A Selective Reagent for Nitrate, Angew. Chem. Int. Ed. 41 (2002) 1416-1419.

[23]. T. Mizuno, W.H. Wei, L.R. Eller, J.L. Sessler, Phenanthroline Complexes Bearing Fused Dipyrrolylquinoxaline Anion Recognition Sites: Efficient Fluoride Anion Receptors, J. Am. Chem. Soc. 124 (2002) 1134-1135.

[24]. F. Sancenon, R. Martinez-Manez, M.A. Miranda, M.J. Segui, J. Soto, Towards the Development of Colorimetric probes to Discriminate between Isomeric Dicarboxylates, Angew. Chem. Int. Ed. 42 (2003) 647-650.

[25]. T. Gunnlaugsson, J.P. Leonard, N.S. Murray, Highly selective colorimetric naked-eye Cu(II) detection using an azobenzene chemosensor, Org. Lett. 6 (2004) 1557-1560.

[26]. T.L. Kao, C.C. Wang, Y.T. Pan, Y.J. Shiao, J.Y. Yen, C.M. Shu, , G.H. Lee, S.M. Peng, W.S.J. Chung, Upper Rim Allyl- and Arylazo-Coupled Calix[4]arenes as Highly Sensitive Chromogenic Sensors for Hg^{2+} Ion, Org. Chem. 70 (2005) 2912-2920.

[27]. S.J. Lippard, J.M. Berg, Principles of Bioorganic Chemistry, University Science Books: Mill Valley, CA, USA, 1994.

[28]. E.L. Que, D.W. Domaille, C.J. Chang, Metals in neurobiology: Probing their chemistry and biology with molecular imaging, Chem. Rev. 108 (2008) 1517-1549.

[29]. D. J. Thielle, A. D. Gitlin, Assembling the pieces, Chem. Biol. 4 (2008) 145-147.

[30]. J. Cho, T. Pradhan, Y.M. Lee, J.S. Kim, S. Kim, A calix[2]triazole[2]arene-based fluorescent chemosensor for probing the copper trafficing pathway in wilson's disease, Dalton Trans. 43 (2014) 16178-16182.

[31]. G.R. You, G.J. Park, J.J. Lee, C. Kim, A colorimetric sensor for the sequential detection of Cu^{2+} and CN^{-} in fully aqueous media: Practical performance of Cu^{2+}, Dalton Trans. 44 (2015) 9120-9129.

[32]. M. Bonham, M. Jacqueline, M.H. Bernadette, J.J. Strain, The immune system as a physiological indicator of marginal copper status, J. Nutr. 87 (2002) 393-403.

[33]. D. Rakel, Integrative Medicine, 2nd ed., Saunders Elsevier, Philadelphia, 2007.

[34]. C.D. Davis, Low Dietary Copper Increases Fecal Free Radical Production, Fecal Water Alkaline Phosphate Activity and Cytotoxicity in Healthy Men, J. Nutr. 133 (2003) 522-527.

[35]. K.J. Barnham, C.L. Masters, A.I. Bush, Neurodegenerative diseases and oxidative stress, Nat. Rev. 3 (2004) 205-214.

[36]. L.M. Gaetke, C.K. Chow, Copper toxicity, oxidative stress, and antioxidant nutrients, Toxicology. 189 (2003) 147-163.

[37]. D.J. Waggoner, T.B. Bartnikas, J.D. Gitlin, The role of copper in neurodegenerative disease, Neurobiol. Dis. 6 (1999) 221-230.

[38]. P. Zatta, A. Frank, Copper deficiency and neurological disorder in man and animal, Res. Rev. 54 (2007) 19-33.

[39]. E.J. Van Genderer, A.C. Ryan, J.R. Tomasso, J.K. Klaine Evaluation of acute copper toxicity to larval fathead minnows (pimephales promelas) in soft surface waters, Environ. Toxicol. Chem. 24, 408-414.

[40]. J.K. Mclntyre, D.H. Baldwin, J.P. Meador, N.L. Scholz, Chemosensory deprivation in juvenile coho salmon exposed to dissolved copper under varying water chemistry condition, Environ. Sci. technol. 42 (2008) 1352-1358.

[41]. Lead and Copper Rule Compliance Help for Public Water Systems-EPA, 2017 <https://www.epa.gov/dwreginfo/lead-and-coppeer-rule-compliance-help-primacy agencies/> (Accessed 23 March 2017).

[42]. B. Halliwell, J. M. C. Gutteridge, Free radicals in Biology and Medicine 3 Oxford University Press, Canada, 1999.

[43]. S.K. Mondal, G. Chakraborty, M. Gupta, U.K. Mazumder, In vitro antioxidant activity of Diospros malabarica Kostel bark, Indian J. Exp. Biol., 44 (2006) 39-44.

[44]. M. Irshad, P.S. Chaudhuri, Oxidant-antioxidant system: role and significance in human body, Indian J. Exp. Biol., 40 (2002) 1233-1239.

[45]. K. L. Liao, M. C. Yin, Individual and Combined Antioxidant Effects of Seven Phenolic Agents in Human Erythrocyte Membrane Ghosts and Phosphatidylcholine Liposome Systems: Importance of Partition Coefficient, J. Agric. Food Chem. 48 (2000) 2266-2270.

[46]. B. Halliwell, The biomarker concept, Nutr. Rev. 57 (1999) 104-113.

[47]. Y.-J. Wu, C.-Y. Hong, S.-J. Lin, P. Wu, M.-S. Shiao, Increase of Vitamin E content in LDL and Reduction of Atherosclerosis in Cholesterol-Fed Rabbits by a Water-Soluble Antioxidant-Rich Fraction of Salvia miltiorrhiza, Arterioscler. Thromb. Vasc. Biol., 18 (1998) 481-486.

[48]. U. Bandyopadhyay, A. Das, R.K. Bannerjee, Reactive oxygen species: Oxidative damage and pathogenesis, Curr. Sci. 5 (1999) 658-666.

[49]. I. S. Young, I. V. Woodside, Antioxidants in health and disease, J. Clin. Pathol. 54 (2001) 176-186.

[50]. S. B. Kedare, R. P. Singh, Genesis and development of DPPH method of antioxidant assay, J. Food Sci. Technol. 48 (2011) 412-422.

[51]. T. Peters (Jr.) all about Albumins: Biochemistry, Genetics and Medical Applications; Academic Press: San Diego, 1996.

[52]. J. F. Foster Albumin Structure, Fuction and Uses; Pregamon Press: Oxford, 1977.

[53]. M. Shyamal, P. Mazumdar, S. Maity, G. P. Sahoo, G. Salgado-Moran, A. Misra, Pyrene scaffold as real-time fluorescent turn-on chemosensor for selective detection of trace-level Al(III) and its aggregation-induced emission enhancement, J. Phys. Chem. A, 120 (2016) 210-220.

[54]. D. Roy, A. Chakraborty, R. Ghosh, Perimidine based selective colorimetric and fluorescent turn-off chemosensor of aqueous Cu2+: studies on its antioxidant property along with its interaction with calf thymus-DNA, RSC Adv. 7 (2017) 40563-40570.

[55]. W.-L. Wang, D.-L. Yang, L.-X. Gao, C.-L. Tang, W.-P. Ma, H.-H. Ye, S.-Q. Zhang, Y.-N. Zhao, H.-J. Xu, Z. Hu, X. Chen,W.-H. Fan, H.-J. Chen, J.-Y. Li, F.-J. Nan, J. Li, B. Feng, 1*H*-2,3-Dihydroperimidine Derivatives: A New Class of Potent Protein Tyrosine Phosphatase 1B Inhibitors, Molecules 19 (2014) 102-121.

[56]. S. Das, S. Parveen, A.B. Pradhan, An insight into the interaction of phenanthridine dyes

with polyriboadenylic acid: spectroscopic and thermodynamic approach, Spectrochim. Acta Part A: Mol. Biomol. Spectrosc. 118 (2014) 356–366.

[57]. W. H. Melhuish, Quantum efficiencies of fluorescence of organic substances: effect of solvent and concentration of the fluorescent solute[1], J. Phys. Chem. 65 (1961) 229-235.

[58]. D. F. Eaton, Reference material for fluorescent measurement, Pure Appl. Chem. 60 (1988) 1107-1114.

[59]. H.A. Benesi, J.H. Hildebrand, A spectrophotometric investigation of the interaction of iodine with aromatic hydrocarbons, J. Am. Chem. Soc. 71 (1949) 2703-2707.

[60]. P. Job, Formation and stability of inorganic complexes in solution, Ann. Chim. Appl. 9 (1928) 113-203.

[61]. A.F. Pozharskii, G.G. Yurchuk, L.L. Gervits, Heterocyclic analogs of pleiadiene. 41. Synthesis of 2-perfluoroalkyl perimidines, Chem. Heterocycl. Compd. 15 (1979) 342-345.

[62]. J. Chen, C.C.W. Law, J.W.Y. Lam, Y. Dong, S.M.F. Lo, I.D. Williams, D. Zhu, B.Z. Tang, Synthesis, light emission, nanoaggregation, and restricted intramolecular rotation of 1,1-substituted 2,3,4,5-tetraphenylsiloles, Chem. Mater. 15 (2003) 1535-1546.

[63]. R. Hu, E. Lager, A. Aguilar-Aguilar, J. liu, J.W.Y. Lam, H.H.Y. Sung, I.D. Williams, Y. Zhong, K.S. Wong, E. Pena-Caberera, Twisted intramolecular charge transfer and aggregation-induced emission of BODIPY derivatives, J. Phys. Chem. C 113 (2009) 15845-15853.

[64]. N.I. Nijegorodov, W.S. Downey, The influence of planarity and rigidity on the absorption and fluorescence parameters and intersystem crossing rate constant in aromatic molecules, J. Phys. Chem. 98 (1994) 5639-5643.

[65]. V.V. Prokhorov, S.I. Pozin, D.A. Lypenko, O.M. Perelygina, E.I. Maltsev, A.N. Vannikov, Molecular arrangements in two-dimensional *J*-aggregate monolayers of cyanine dyes, Macroheterocycles 5 (2012) 371-376.

[66]. O. Garcia-Beltran, B.K. Cassels, C. Perez, N. Mena, M.T. Nunez, N.P. Martinez, P. Parvez, M.E. Aliaga, Coumarim-based fluorescent probes for dual recognition of copper (II) and iron (III) ions and their application in bio-imaging, Sensors 14 (2014) 1358-1371.

[67]. D. Udhayakumari, S. Velmathi, Y.-M. Sung, S.-P. Wu, Highly fluorescent probe for copper (II) ion based on commercially available compounds and live cell imaging, Sens. Actuator B-Chem. 198 (2014) 285-293.

[68]. H.-F. Wang, S.-P. Wu, A pyrene-based highly selective turn-on fluorescent sensor for copper (II) ions and its application in living cell imaging, Sens. Actuator B-Chem. 181 (2013) 743-748.

[69]. M. Salpem, K.H. Lee, Selective fluorescence detection of Cu^{2+} in aqueous solution and living cells, J. Lumin. 145 (2014) 843-848.

[70]. D. Li, M. Zhu, C. Xu, J.J. Chen, B. Ji, The effect of Cu^{2+} or Fe^{2+} on the noncovalent binding of Rutin with bovine serum albumin by spectroscopic analysis, Spectrochim. Acta A 78 (2011) 74-79.

[71]. X. Li, D. Chen, G. Wang, Y. Lu, Investigation on the interaction between bovine serum albumin and 2,2-Diphenyl-1-picryl hydrazyl, J. Lumin. 156 (2014) 255-261.

[72]. E.A. Brustein, N.S. Vedenkina, M.N. Ivkova, Fluorescence and the location of tryptophan residues in protein molecules, Photochem. Photobiol. 18 (1973) 263-279.

[73]. J.R. Lakowicz, Principles of fluorescence spectroscopy, Pherum press: New York, 2006.

Graphical Abstract

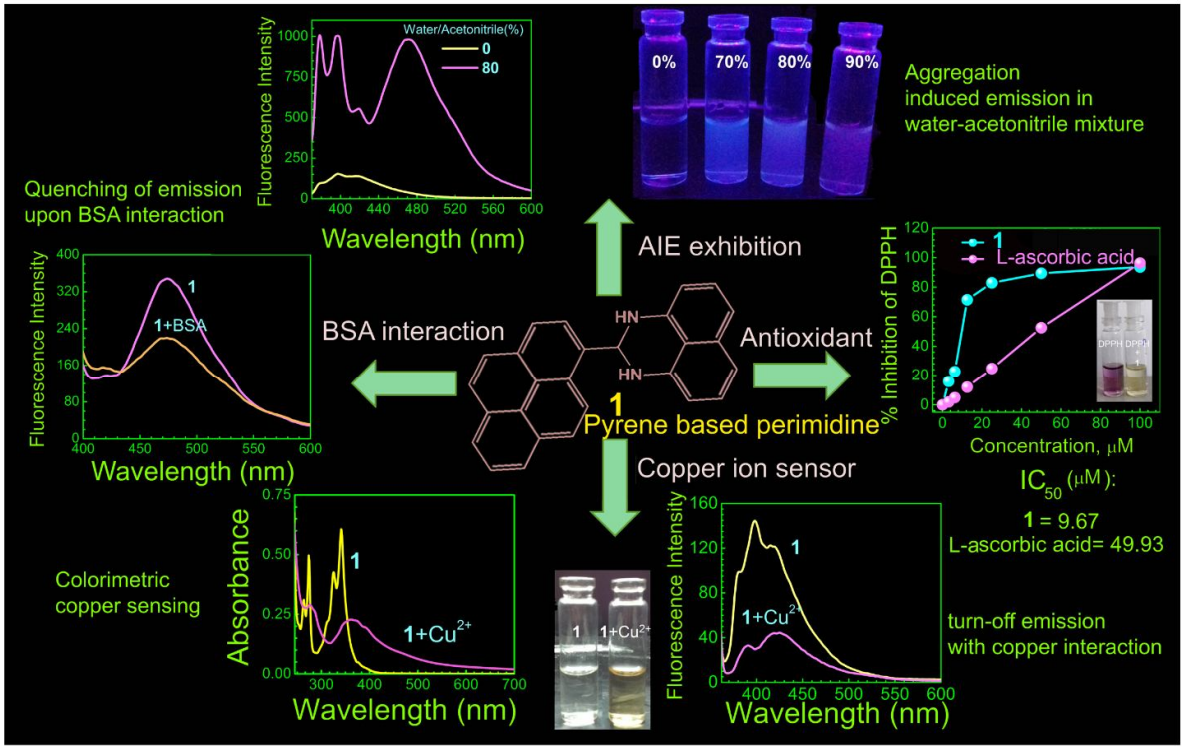

Supplementary Information

Synthesis of a novel pyrene derived perimidine and exploration of its aggregation induced emission, aqueous copper ion sensing, effective antioxidant and BSA interaction properties

Nilanjan Chakraborty[a,b], Sejuti Banik[b], Arijit Chakraborty[c*], Swapan Kumar Bhattacharya[b], Suman Das[b*]

[a]Department of Chemistry, Maulana Azad College 8, Rafi Ahmed Kidwai Road, Kolkata 700 013, India.

[b]Department of Chemistry, Jadavpur University, Kolkata 700 032, India.

[c]Department of Chemistry, Acharya B N Seal College, Cooch Behar, West Bengal 730 161, India.

*Corresponding Authors

To whom all correspondence should be addressed.

Suman Das

Department of Chemistry

Jadavpur University

Raja S. C. Mullick Road, Jadavpur

Kolkata 700 032; India

Tel.: +91 94 3437 3164, +91033 2457 2349

Fax: +91 33 2414 6266

E-mail: sumandas10@yahoo.com

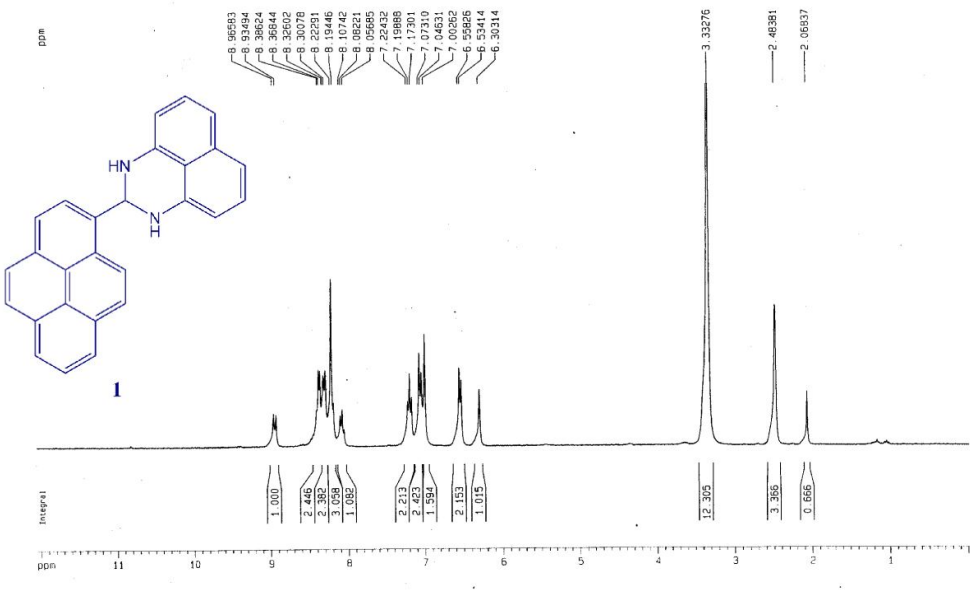

Fig. S1

Fig. S1. ^{1}H-NMR spectrum of **1** in d^{6}-DMSO.

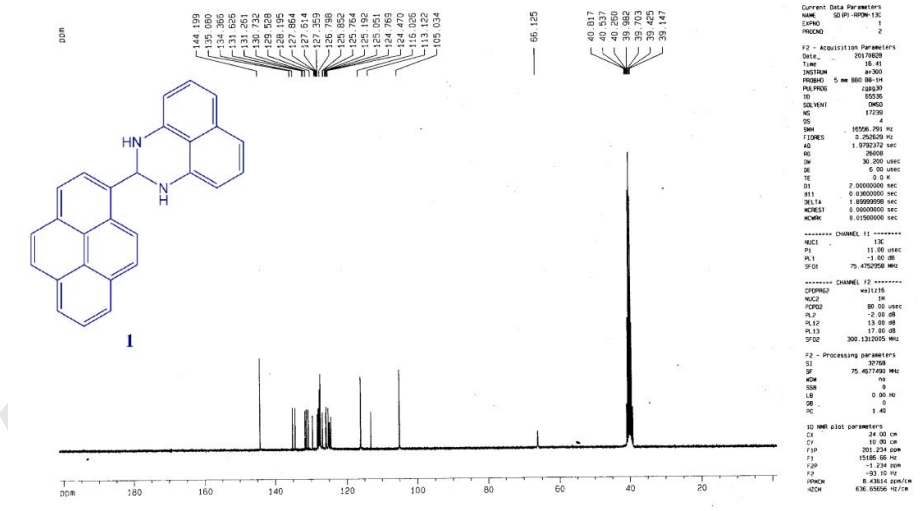

Fig. S2

Fig. S2. ^{13}C-NMR spectrum of **1** in d^{6}-DMSO.

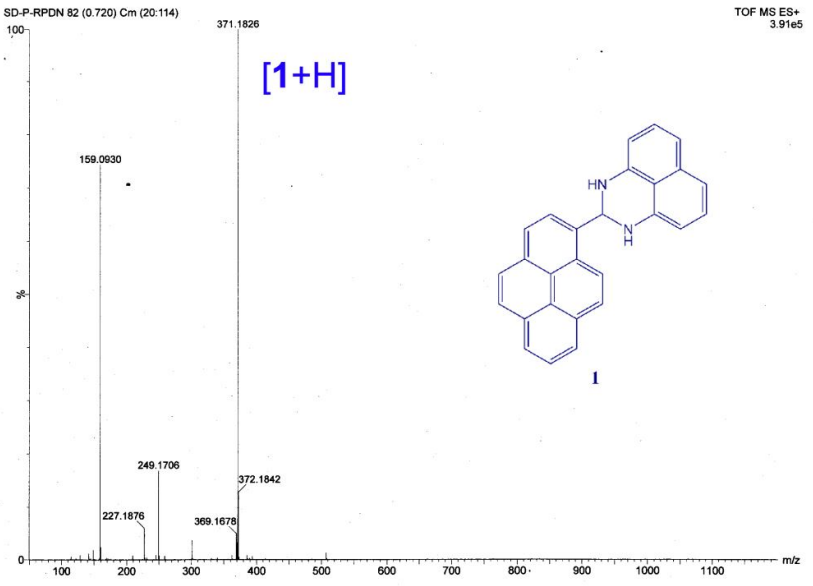

Fig. S3

Fig. S3. HRMS spectrum of **1**.

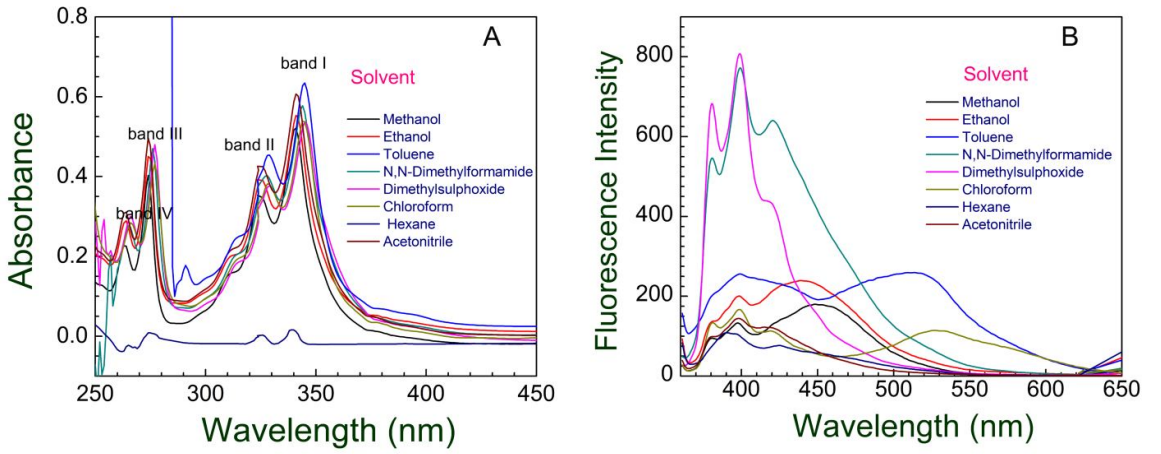

Fig. S4

Fig. S4. A) Solvent effect on absorption spectrum of **1** (10μM). B) Solvent effect on emission spectrum of **1** (10μM).

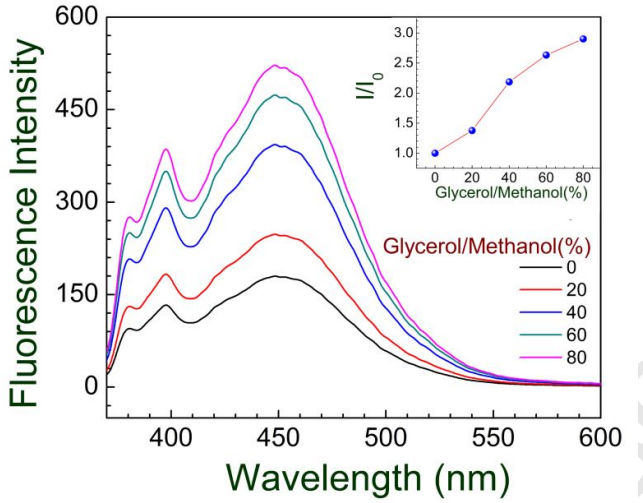

Fig. S5

Fig. S5. Effect of viscosity on emission spectrum of fluorophore **1** (10μM).

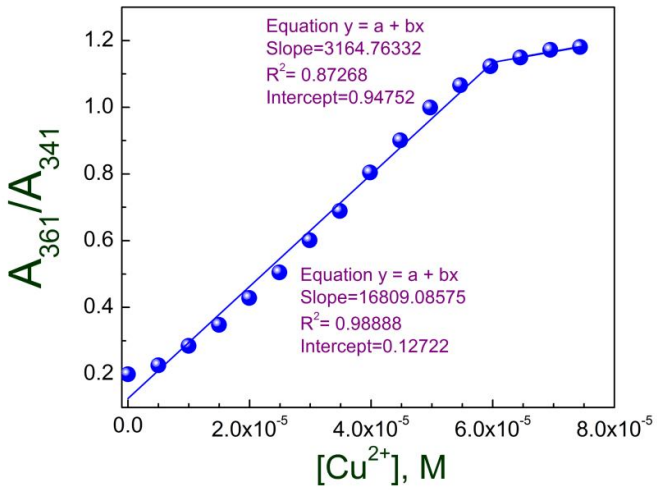

Fig. S6

Fig. S6. Calibration curve for variation of ratiometric absorbance of sensor **1**(10 μM) at 361nm to 341nm with concentration of analyte Cu^{2+}.

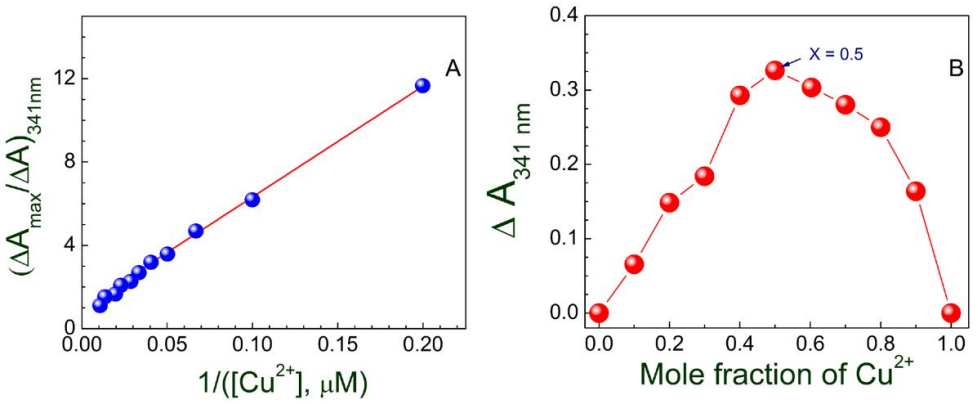

Fig. S7

Fig. S7. A) Benisi-Hildebrand plot from absorption titration profile of **1** with aqueous Cu^{2+} in acetonitrile. B) Jobs plot for complexation of **1** with Cu^{2+}.

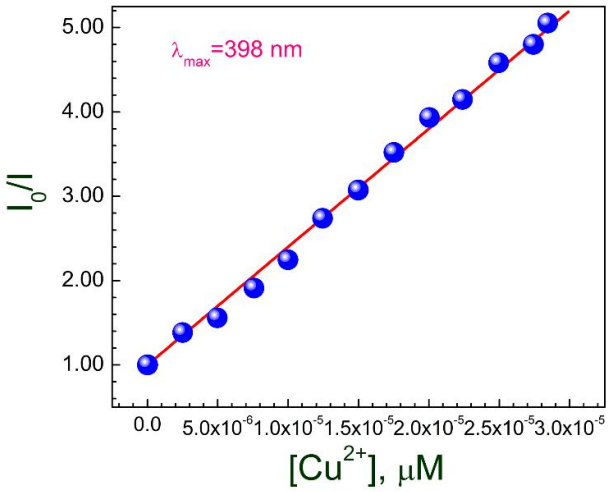

Fig. S8

Fig. S8. Stern-Volmer quenching plot of relative fluorescence intensity with variation of Cu^{2+} concentration.

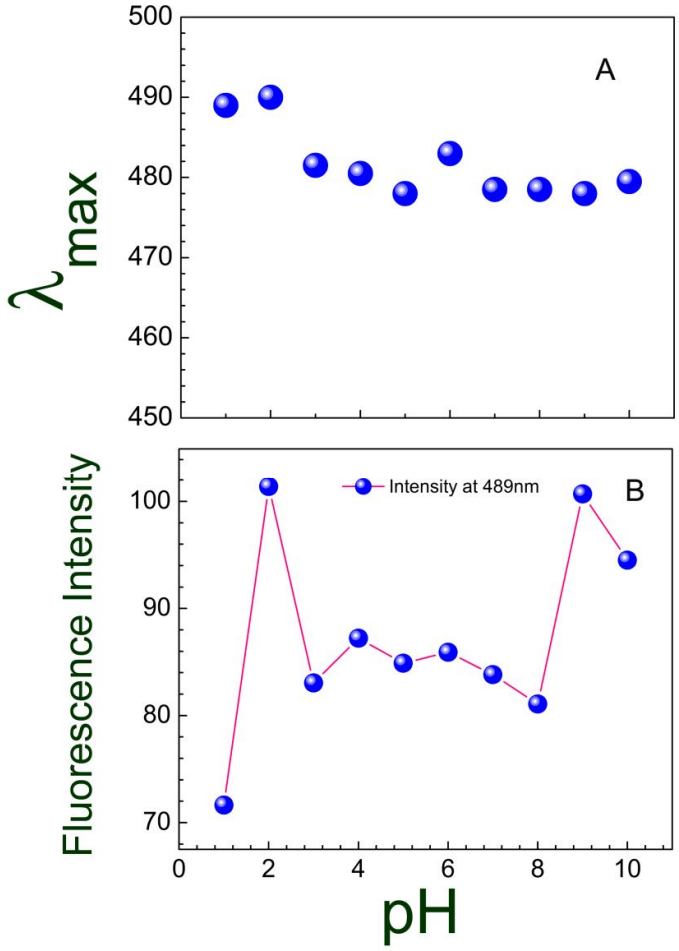

Fig. S9

Fig. S9. A) Effect of pH on shift in wavelength in emission spectrum of fluorophore **1** (10μM). B) Effect of pH on increase in relative intensity in emission spectrum of fluorophore **1** (10μM).

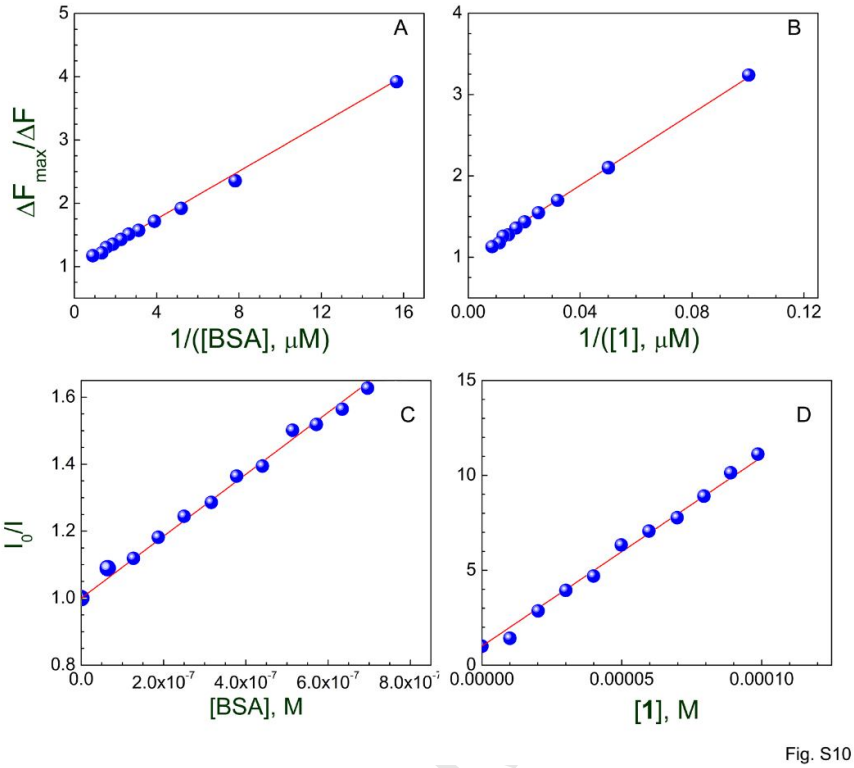

Fig. S10

Fig. S10. A) Benisi-Hildebrand plot at 474nm from emission titration profile of **1** with BSA. B) Benisi-Hildebrand plot at 348nm from emission titration profile of BSA with **1**. C) Stern-Volmer quenching plot of relative fluorescence intensity of **1** with variation of BSA concentration. D) Stern-Volmer quenching plot of relative fluorescence intensity of BSA with variation of drug **1** concentration.

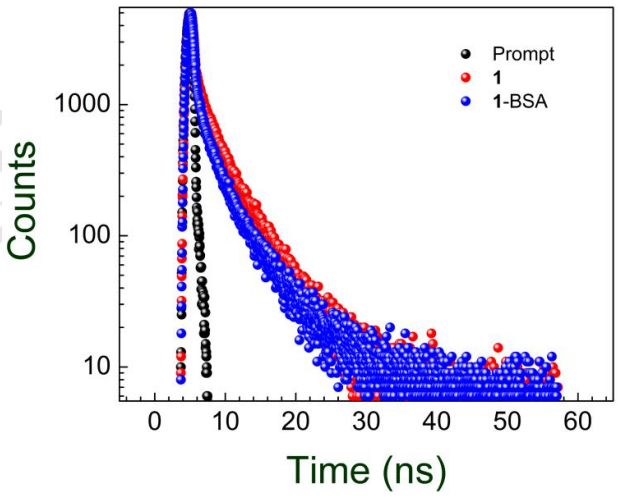

Fig. S11

Fig. S11. Decay profile of free fluorophore **1** and protein bound fluorophore (BSA-**1**) in Tris-HCl buffer.

Tables:

Table S1. Parameters related to UV-vis and emission spectra of compound **1** in various solvents.

Solvent	Dielectric constant (ε) at 20 °C	Absorption bands (nm)	Emission Bands (nm)
Acetonitrile	37.5	341, 325, 274, 264	380, 398, 415
Dimethl formamide	36.7	344, 329, 291, 287	380.5, 399, 420.5
Chloroform	4.81	344, 328, 277, 266	381, 398.5, 419, 528
Dimethyl sulfoxide	46.7	345, 329, 277, 266	380.5, 399, 419
Ethanol	24.5	341, 325, 274, 264	380, 397.5, 448.5
Methanol	32.7	341, 325, 274, 263	380, 397.5, 448.5
Toluene	2.38	345, 329, 291, 287	380, 399, 513.5
Hexane	1.89	340, 325, 276, 266	380, 395.5, 425

Table S2. Decay parameters of the time resolved study of sensor **1** and **1**+BSA in Tris-HCl buffer medium.

Solutions	τ_1 (ns)	(α_1)	τ_2 (ns)	(α_2)	τ_3 (ns)	(α_3)	χ^2	Average life time (τ) the fluorophore **1** (ns)
1	2.76	0.009	7.99	0.001	0.12	0.207	1.17	0.27
1+BSA	1.86	0.007	5.93	0.002	0.10	0.205	1.19	0.22

Highlights

- A new pyrene derived dihydroperimidine [2-(pyren-1-yl)-2,3-dihydro-1*H*-perimidine] was synthesized where it showed selective naked-eye, absorption and fluorescence spectral responses towards copper (Cu^{2+}) ion in nanomolar level.
- Aggregation induced enhancement in emission intensity of 2-(pyren-1-yl)-2,3-dihydro-1*H*-perimidine was reported and investigated with the help of absorption, fluorescence, life-time and dynamic light scattering experiments.
- Antioxidant property of the pyrene based perimidine was established in comparison to L-ascorbic acid by studying inhibtion of DPPH assay (spectrophotometrically) and by oxidation potentials (cyclic voltammetric studies).
- Interaction of the perimidine with Bovine serum albumin in Tris-HCl buffer.